Appendix A

Regression Versus a Simpler Stress Model

A simpler SVD-based statistical model of wind stress anomalies has been used by several authors (Syu and Neelin, 1995; Blanke et al., 1997; Cassou and Perigaud, 2000). In this model, the stress singular vector expansion coefficients $\widetilde{\mathbf{Y}}^*$ are assumed equal to the SST singular vector expansion coefficients $\widetilde{\mathbf{X}}^*$. This model takes the form

$$\widehat{\mathbf{Y}}_N = \widetilde{\mathbf{X}}^*_N \mathbf{B}'_N \tag{A.1}$$

which essentially replaces the regressed $\boldsymbol{\tau}'$ anomalies in Figs. 3.7–3.8 with the singular vectors of $\boldsymbol{\tau}'$ shown in Fig. 3.5.

A comparison of the regression estimate (3.26) with the estimate (A.1) is shown in Table A.1. For unfiltered stress data, the two models have nearly the same residual variance ("error") of monthly-means. On this basis, it might at first appear that the regression is not much of an improvement over (A.1). However, the regression is superior in several important ways.

First, because the wind stress is noisy, improvements in the deterministic part of the model are hard to discern in the monthly data. Filtering the stress to retain only interannual variations shows that (A.1) gives a mean square error 12% larger than the regression model for these time scales. Presumably these are the time scales most important to ENSO.

More importantly, model (A.1) assumes that the singular mode expansion coefficients are perfectly correlated. In fact, these correlations drop off rapidly after the gravest mode (Fig. A.1). For higher modes, (A.1) will overestimate the influence of SST on the wind stress by nearly a factor of two. This is why the model variance of (A.1) is nearly twice as large as the regression, and why the skill of (A.1) actually gets *worse* as the number of modes increases. Thus an important benefit of the regression (3.26) is its more accurate representation of the air-sea coupling strength.

Finally, from Table A.1 it is clear that the regression model is optimal (in a least squares sense) because the model and residual variances sum to the total variance for the unfiltered data. The regression model is close to optimal for the interannual wind stress as well. That (A.1) fits the data fairly well, even though its variance is so much greater than the optimal estimate, indicates that it is probably an overfit to the data. This problem is even more apparent for the interannual stress anomalies. Thus while (A.1) shows good

Table A.1: Analysis of variance of the 1980–1999 FSU wind stress anomalies for two different models $\widehat{\mathbf{Y}}_N$, both based on $N = 3$ modes. Results are shown for unfiltered data, and for data filtered to retain only periods greater than one year. Variances are expressed as a percentage of the total variance of the wind stress anomalies (40.8 dPa^2 unfiltered, 10.7 dPa^2 interannual). The regression model corresponds to $\widehat{\mathbf{Y}}_N = \widetilde{\mathbf{X}}^*_N \widehat{\mathbf{R}}_N$. The direct SVD model corresponds to $\widehat{\mathbf{Y}}_N = \widetilde{\mathbf{X}}^*_N \mathbf{B}'_N$.

	Regression	Direct SVD
Total $\boldsymbol{\tau}'$		
model variance	13.9	25.1
residual variance	86.1	89.4
sum	100.0	114.5
Interannual $\boldsymbol{\tau}'$		
model variance	41.2	71.5
residual variance	54.8	61.6
sum	96.0	133.1

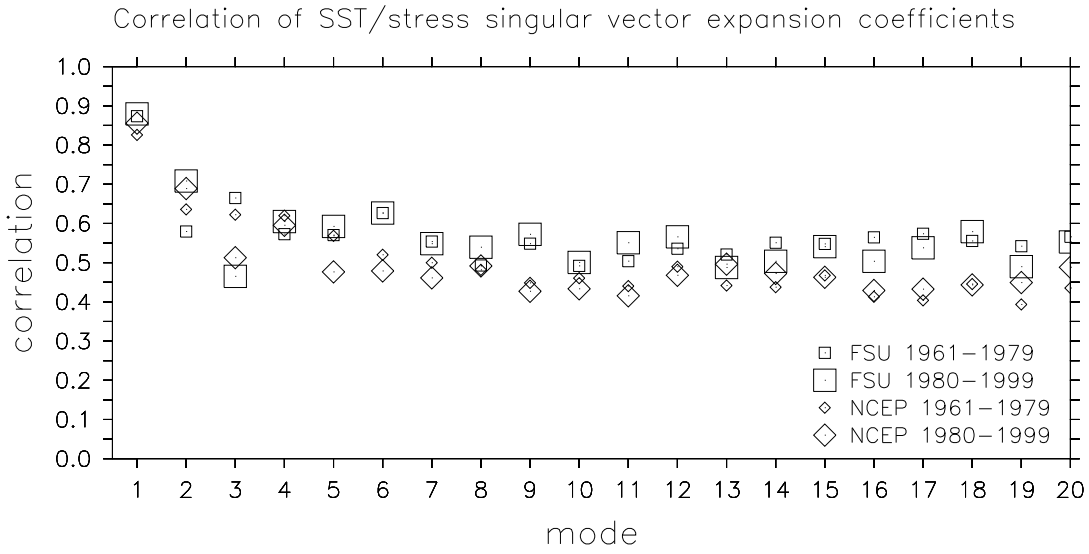

Figure A.1: Correlation of SST singular vector expansion coefficients with stress singular vector expansion coefficients.

skill in reconstructing the training data, it would perform much worse given a different realization of the noise. Obviously the purpose of the model is to forecast the unknown, not the known. Therefore we proceed using the regression estimate (3.26).

Appendix B

Field Significance

To determine the field significance of a collection of local hypothesis tests performed on a grid, one must find the probability of rejecting at least x of the N gridpoints at significance level p, assuming the null hypothesis is true. If this probability is small, then one may confidently reject the null hypothesis, and infer that the field as a whole was not generated by the assumed reference process.

If there were no spatial correlations in the residual, then this problem would be equivalent to finding the probability of x successes in N trials, where the probability of success in any single trial is p. If X is a hypothesized number of successes, then the binomial distribution (Wilks, 1995) gives the probability of observing $X = x$ successes:

$$Pr\{X = x\} = \binom{N}{x} p^x (1-p)^{N-x} \tag{B.1}$$

The probability of *at least* x successes is then

$$Pr\{X \geq x\} = \sum_{i=x}^{N} \binom{N}{i} p^i (1-p)^{N-i} \tag{B.2}$$

$$= 1 - \sum_{i=0}^{x-1} \binom{N}{i} p^i (1-p)^{N-i} \tag{B.3}$$

This probability is shown in Fig. B.1, using unconnected symbols, for the cases of Fig. 3.9 ($N = 324$) and Fig. 3.10 ($N = 513$ for 1961–1979, $N = 540$ for 1980–1999). In each case the probability of "success" is taken to be the local significance level, $p = 0.01$, and the number of trials N is taken to be the number of gridpoints tested.

In the presence of spatial correlation, one can redefine N to be an "effective" number of gridpoints, which decreases as the correlation increases. For the wind stress residual, assuming a conservative zonal decorrelation scale of 40° longitude gives $N \approx 3$. The binomial probabilities associated with this value of N are shown in Fig. 3.9 using symbols connected by lines. The figure indicates that in this spatially-correlated case, roughly two to four times as many points must be rejected by the local significance test to attain field significance.

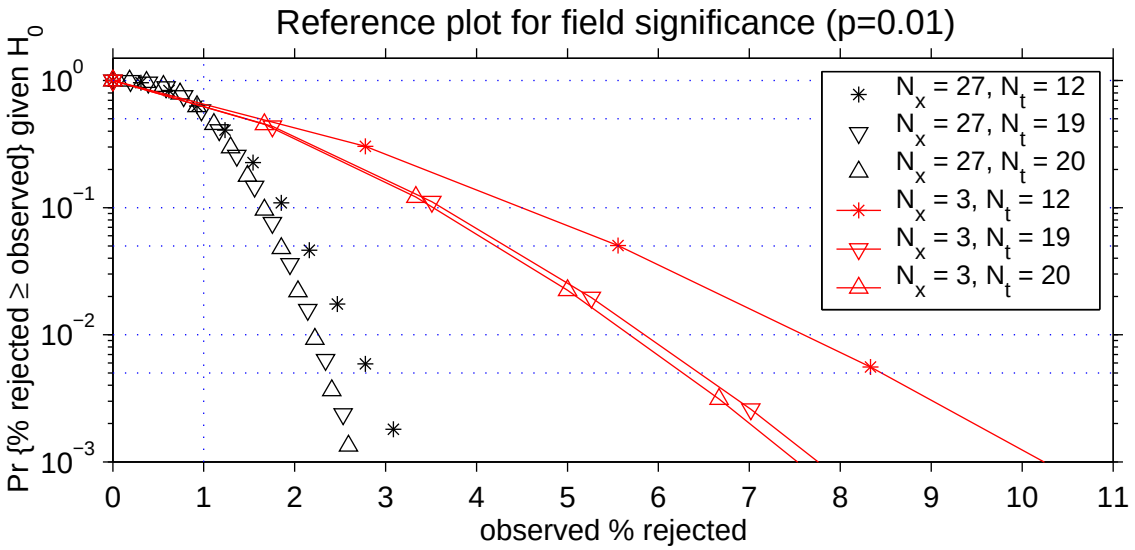

Figure B.1: Reference plot for evaluating field significance of the local hypothesis tests of Figs. 3.9 and 3.10. Abscissa gives the observed percentage of points rejected by the local test at significance level $p = 0.01$. Ordinate gives the binomial probability that the percent rejected could have been greater than or equal to that observed, assuming the null hypothesis were true. Unconnected symbols correspond to the assumption of no spatial correlation, such that $N_x = 27$ is the number of zonal gridpoints. Line-connected symbols correspond to an assumed zonal decorrelation scale of 40° longitude, such that the effective number of zonal gridpoints is $N_x = 3$. Asterisks ($N_t = 12$) correspond to the 12 calendar months of Fig. 3.9. Triangles ($N_t = 19$ and $N_t = 20$) correspond to the years 1961–1979 and 1980–1999 in Fig. 3.10.

Appendix C

Upwelling in the Intermediate Model

In the intermediate model, upwelling at the base of the mixed layer is given by the divergence of mixed layer transport (4.10):

$$w = \nabla \circ \mathbf{U} \tag{C.1}$$

where from (4.17),

$$\mathbf{U} = \mathbf{U}_s + \frac{H_m}{H}\left(\mathbf{U}_{al} - \mathbf{U}_s\right) \tag{C.2}$$

The divergence of the active-layer transport is given by (4.3) and (4.7)–(4.8):

$$\boldsymbol{\nabla} \circ \mathbf{U}_{al} = -\frac{\lambda_u}{\lambda_h}(\partial_t h + rh) \tag{C.3}$$

The Ekman transport is given by (4.15):

$$\mathbf{U}_s = \frac{r_s \boldsymbol{\tau} - f\hat{k} \times \boldsymbol{\tau}}{\rho\left(f^2 + r_s^2\right)} \tag{C.4}$$

Solving (C.1)–(C.4) for w away from boundaries gives

$$\begin{aligned} w = \; & - \; \frac{H_m \lambda_u}{H \lambda_h}(\partial_t h + rh) \\ & + \; \frac{H - H_m}{\rho H (f^2 + r_s^2)}\left[r_s \mathrm{div}(\boldsymbol{\tau}) + f\mathrm{curl}(\boldsymbol{\tau}) + \frac{\beta(f^2 - r_s^2)\tau_x - 2\beta f r_s \tau_y}{f^2 + r_s^2}\right] \end{aligned} \tag{C.5}$$

The first term arises from the shallow water dynamics and is quite small, on the order of 0.05 m day^{-1} for standard parameter values. The remaining terms immediately suggest a rescaling of y:

$$\tilde{y} \equiv \frac{\beta}{r_s} y = \frac{f}{r_s} \tag{C.6}$$

Dropping the first term in (C.5) and substituting for y then gives

$$w = \frac{H - H_m}{\rho H(\tilde{y}^2 + 1)}\left[\frac{\mathrm{div}(\boldsymbol{\tau})}{r_s} + \frac{\tilde{y}\mathrm{curl}(\boldsymbol{\tau})}{r_s} + \frac{\beta}{r_s^2}\left(\frac{\tilde{y}^2 - 1}{\tilde{y}^2 + 1}\tau_x - \frac{2\tilde{y}}{\tilde{y}^2 + 1}\tau_y\right)\right] \tag{C.7}$$

It is enlightening to examine this solution at three key latitudes:

$$w(\tilde{y}=0) = \frac{H-H_m}{\rho H}\left(\frac{\mathrm{div}(\boldsymbol{\tau})}{r_s} - \frac{\beta\tau_x}{r_s^2}\right) \tag{C.8}$$

$$w(\tilde{y}=\pm 1) = \frac{H-H_m}{2\rho H}\left(\frac{\mathrm{div}(\boldsymbol{\tau})}{r_s} \pm \frac{\mathrm{curl}(\boldsymbol{\tau})}{r_s} \mp \frac{\beta\tau_y}{r_s^2}\right) \tag{C.9}$$

$$w(|\tilde{y}| \gg 1) = \frac{H-H_m}{\rho H}\frac{\mathrm{curl}(\boldsymbol{\tau})}{r_s\tilde{y}} \tag{C.10}$$

In all three cases, the upwelling increases as H_m shoals relative to H. Equation (C.8) indicates that at the equator, upwelling is generated both by stress divergence and by easterly stress, with the latter effect usually dominating. The viscosity parameter r_s exerts a strong control over the equatorial upwelling, with w scaling like r_s^{-2}. Equation (C.9) indicates that at $y = r_s\beta^{-1}$, the direct effect of the easterlies vanishes; here the upwelling is generated by stress divergence, cyclonic stress curl, and equatorward stress. To the extent that the wind stress is large in scale, (C.9) indicates that the meridional winds will be important for generating upwelling slightly away from the equator, with the strength of the upwelling scaling like r_s^{-2}. Finally, (C.10) indicates that upwelling far from the equator is entirely due to the wind stress curl; this upwelling decreases with increasing r_s and increasing latitude.

It is interesting to compare the effects of easterlies versus southerlies. For spatially constant easterlies, (C.7) becomes

$$w = \frac{\beta}{\rho r_s^2}\frac{H-H_m}{H}\frac{\tilde{y}^2-1}{(\tilde{y}^2+1)^2}\,\tau_x \tag{C.11}$$

The upwelling zone extends to $y = \pm r_s\beta^{-1}$, and so widens with increasing r_s. Integrating over the latitudes of upwelling gives

$$\int_{-1}^{1} w\,d\tilde{y} = -\frac{\beta}{\rho r_s^2}\frac{H-H_m}{H}\,\tau_x \tag{C.12}$$

For spatially constant southerlies, on the other hand, (C.7) becomes

$$w = \frac{\beta}{\rho r_s^2}\frac{H-H_m}{H}\frac{-2\tilde{y}}{(\tilde{y}^2+1)^2}\,\tau_y \tag{C.13}$$

The upwelling is a maximum at $y = -3^{-1/2}r_s\beta^{-1}$. Integrating over the latitudes of upwelling gives

$$\int_{-\infty}^{0} w\,d\tilde{y} = \frac{\beta}{\rho r_s^2}\frac{H-H_m}{H}\,\tau_y \tag{C.14}$$

Comparison of (C.12) and (C.14) shows that for equal magnitudes of wind stress, *southerlies* induce as much total upwelling *south* of the equator as *easterlies* do *straddling* the equator. South of $y = (1-2^{1/2})r_s\beta^{-1}$, southerlies induce stronger upwelling than easterlies of equal magnitude.

Appendix D

Flux Correction

In the present study we rely on coupled anomaly models, i.e. models in which the climatology in the control run is flux-corrected. It should be noted that Neelin and Dijkstra (1995) have found important dynamical differences between fully-coupled and flux-corrected climatologies. In the latter case, the climatology cannot respond to changes in air-sea coupling, and so as coupling increases the flux-corrected trade winds become too weak relative to the fully-coupled case. These "spurious westerlies" in the flux-corrected case can allow spurious climate equilibria to exist, which can then affect the model variability.

The present model shows a warm equilibrium at high coupling in the absence of noise (Fig. 4.25), which may well be an artifact of the flux correction. That the remnants of this fixed point at lower coupling may interact with the model's stochastic variability can be inferred from Fig. 4.30, which shows the model SST anomalies have negative skewness, i.e. a tendency to linger in warm states. The hybrid GCM, which is also an anomaly model, shows this negative skewness as well (Fig. 7.26). Observed SST anomalies, on the other hand, show positive skewness (Figs. 2.14 and Fig. 2.15).

Unfortunately, it is difficult to maintain a realistic climatology in the present intermediate model without flux correction. There are two main problems. First, the shallow-water model is linear, and so cannot simultaneously simulate both the climatological thermocline's zonal mean depth (which determines the speed of internal waves, and the sensitivity of the thermocline slope to wind stress changes) and its depth in the eastern Pacific (which is crucial to ENSO coupled feedbacks). To simulate a fully-coupled climatology in the present model would require $H = H_0$, which would weaken the wind-thermocline coupling relative to observations. In the flux-corrected case, however, we may achieve a realistic climatological thermocline (Fig. 4.5) without sacrificing realistic wave speed and thermocline sensitivity (Fig. 4.4).

The second problem in simulating a fully-coupled climatology is that many climate processes, such as those involving clouds, evaporation, and vertical mixing, are heavily parameterized in the intermediate model and in the HGCM. Although these parameterizations may be reasonable for simulating ENSO variability, they give rise to errors in simulating the climatology which are then strongly amplified by coupled feedbacks. Prescribing the climatological winds from observations circumvents this problem, allowing us to escape the chain of feedbacks which leads to climate drift.

We have therefore opted for flux correction as a way to obtain a realistic climatology. The concerns noted by Neelin and Dijkstra (1995) are valid but difficult to address directly. Indeed, a prime motivation for the present study is the inability of even many state-of-the-art GCMs to achieve a realistic climatology in the absence of flux correction (Fig. 1.4).

Appendix E

Interval Estimate for the Predictive Power

It is possible to give an interval estimate for the predictive power (PP) under the assumption of univariate normal state vectors. Given (4.32) and the discussion afterward, the quantity

$$\chi^2_{N-1} \equiv \frac{(N-1)s^2}{\sigma^2} \tag{E.1}$$

follows a chi-square distribution on $N-1$ degrees of freedom. Similarly, the quantity

$$\chi^2_{N_c-1} \equiv \frac{(N_c-1)s_c^2}{\sigma_c^2} \tag{E.2}$$

follows a chi-square distribution on $N_c - 1$ degrees of freedom. The ratio of chi-square variables

$$\begin{aligned} F_{N-1,N_c-1} &\equiv \frac{\chi^2_{N-1}/(N-1)}{\chi^2_{N_c-1}/(N_c-1)} \\ &= \frac{s^2/s_c^2}{\sigma^2/\sigma_c^2} \end{aligned} \tag{E.3}$$

then follows an F distribution on $N-1$ and N_c-1 degrees of freedom. By definition of the F-distribution quantiles $F_{N-1,N_c-1,\alpha/2}$ and $F_{N-1,N_c-1,1-\alpha/2}$ we have

$$P\left\{F_{N-1,N_c-1,\alpha/2} < F_{N-1,N_c-1} < F_{N-1,N_c-1,1-\alpha/2}\right\} = 1-\alpha \tag{E.4}$$

which implies

$$P\left\{\frac{s^2/s_c^2}{F_{N-1,N_c-1,1-\alpha/2}} < \frac{\sigma^2}{\sigma_c^2} < \frac{s^2/s_c^2}{F_{N-1,N_c-1,\alpha/2}}\right\} = 1-\alpha \tag{E.5}$$

Substituting from (4.33) then gives a $1-\alpha$ confidence interval for the PP:

$$P\left\{1 - \frac{s/s_c}{F^{1/2}_{N-1,N_c-1,\alpha/2}} < \mathrm{PP} < 1 - \frac{s/s_c}{F^{1/2}_{N-1,N_c-1,1-\alpha/2}}\right\} = 1-\alpha \tag{E.6}$$

Appendix F

Hybrid Coupled GCM

The hybrid GCM used in this study consists of an ocean general circulation model coupled to a statistical model of the surface wind stress and heat fluxes, as in Harrison et al. (2002). Relevant details from that paper are repeated here for convenience, with an additional description of the model climatology and interannual variability.

F.1 Ocean model

The ocean component is the GFDL Modular Ocean Model (MOM) version 3. The horizontal domain of the model, shown in Fig. F.1, extends from 120°E–70°W, 40°S–40°N, with a sponge condition within 10° of the northern and southern boundaries. The zonal grid spacing is a uniform 1°. The meridional grid spacing is a uniform 0.33° below 10° latitude, gradually increases between 10° and 15° latitude, and is a uniform 1° poleward of 15° latitude. The model has 16 fixed vertical levels, with 10 in the top 250 m of the ocean; the vertical grid spacing increases with depth as shown in Fig. F.2. A rigid lid is assumed at the ocean surface. The primitive equations are solved on an Arakawa B grid and advection is computed using centered differences. Vertical mixing is the Richardson number dependent scheme of Pacanowski and Philander (1981); horizontal mixing is the nonlinear scheme of Smagorinsky (1963).

Starting from a resting state with observed temperature and salinity (Levitus and Boyer, 1994), the ocean model is spun up for 25 years using observed climatological monthly surface fluxes of momentum and heat. The surface wind stresses are converted from the FSU pseudostress product (Stricherz et al., 1997), using an air density of $\rho_a = 1.2$ kg m^{-3} and a drag coefficient of $c_d = 1.2 \times 10^{-3}$. Outside the 30°S–30°N domain of FSU, the stresses are taken from Hellerman and Rosenstein (1983). The heat fluxes consist of the OSU analysis (Esbensen and Kushnir, 1981), with an additional restoring of the top level toward observed SST at a rate of 50 Watt m^{-2} °C^{-1}. Surface salinities are restored toward their observed climatological values at a rate 0.01 kg m^{-2} s^{-1} PSU^{-1}. The restoring for the top model level temperature and salinity corresponds to an e-folding time scale of approximately 5 days.

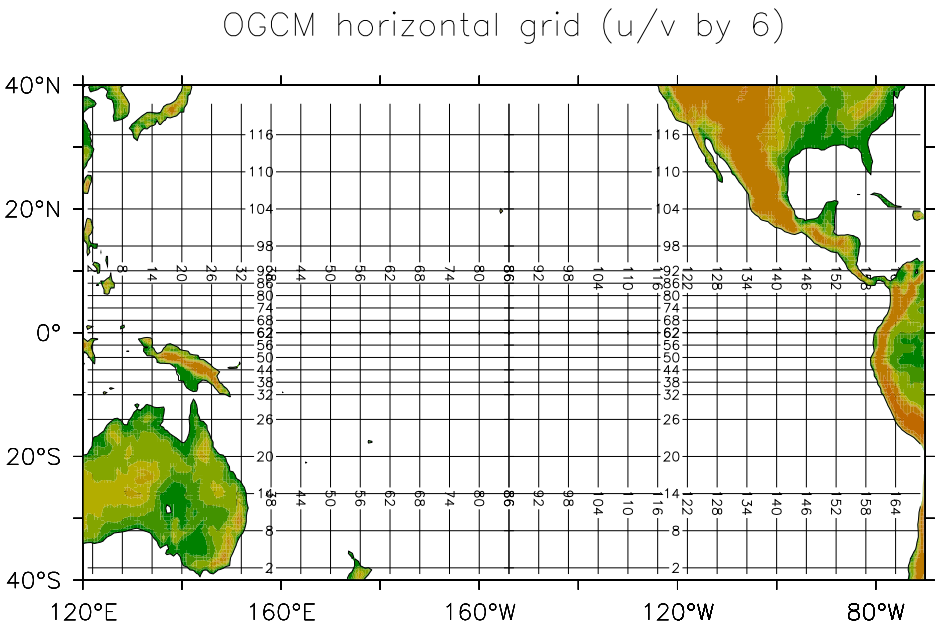

Figure F.1: Horizontal velocity grid of the ocean general circulation model. Gridpoints lie at the line intersections; only every sixth row and column of points is plotted. The temperature and vertical velocity lie on a grid staggered in latitude and longitude with respect to the grid shown.

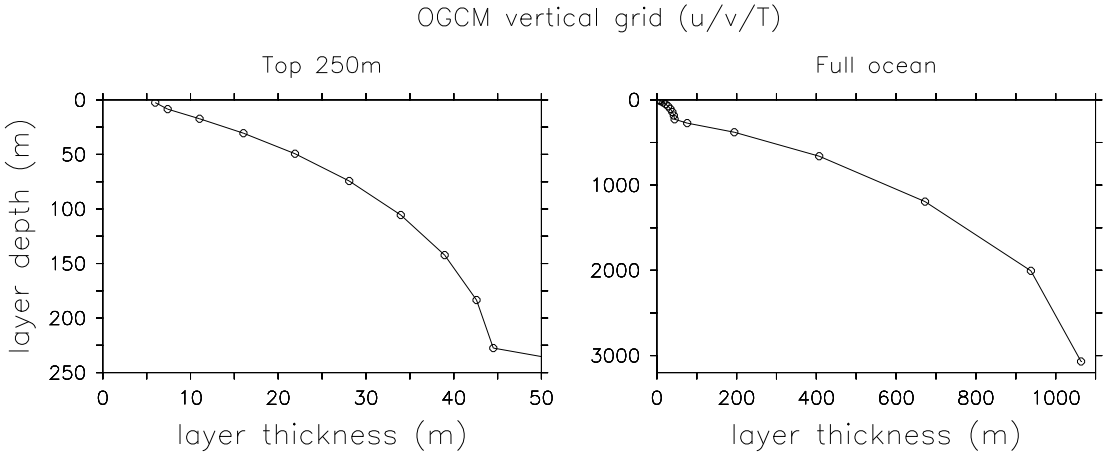

Figure F.2: Vertical grid of the ocean general circulation model. Gridpoints of temperature and horizontal velocity lie at the depths indicated by the circles; layer thicknesses are indicated on the horizontal axis. The vertical velocity grid is staggered in the vertical with respect to the grid shown.

F.2 Statistical atmosphere model

The statistical atmosphere model is very similar to the stress models developed in Chapter 3. Wind stress, latent heat flux, radiative heat flux models are each developed separately (sensible and freshwater fluxes are not included). Harrison et al. (2002) compared several such models based on different flux analyses; here we use the version based on the 1979–1993 period from the ECMWF product (Gibson et al., 1997). SST data are taken for the same period from the analysis of Reynolds and Smith (1994).

The data fields are first interpolated onto a $3^\circ \times 3^\circ$ grid covering the ocean between 20°S–20°N. Monthly climatologies are subtracted from the data to give monthly anomalies, which are then detrended by removing the least-squares linear fit to the timeseries at each gridpoint. As in Chapter 3, the flux models are constructed by performing linear regressions of the observed anomalies onto the leading singular vector patterns of observed flux/SST covariance. Only the gravest regression mode is included in this case, and there is no stochastic component.

F.3 Coupled model

Following the spinup of the ocean climatology, the ocean GCM is coupled to the statistical atmosphere anomaly model. The ocean model climatology is maintained by the imposition of the climatology of restoring terms simulated during the last 10 years of ocean spinup. An additional heat flux is also imposed to damp SST anomalies at a rate of 1 Watt m^{-2} $^\circ C^{-1}$, which corresponds approximately to a restoring time scale of 100 days for the top model layer.

The coupled simulation is initialized with a perturbation from the model climatology, and then is integrated forward in time for 20 years, with output of monthly-average fields. The first four years of the run are considered a transition to the coupled statistical equilibrium and are discarded; only the last 16 years are analyzed. A 12-month climatology is computed from these 16 years of data, and then subtracted from the total fields to give monthly anomaly fields.

F.3.1 Climatology

Annual mean

The annual-mean equatorial temperature structure of the coupled model is shown in Fig. F.3. The simulated ocean is about 1–2°C too cold near the surface in the central and eastern Pacific, and slightly too cold in the western Pacific. Thus $\partial_z T$ is too weak at 50 m depth in the east and the zonal SST gradient is somewhat too strong. The model also has a 2–4°C cold bias below 160 m. These problems are likely related to limitations of the vertical mixing scheme, and perhaps also to errors in the climatological stress forcing, since this forcing is rather uncertain (see Chapter 2). However, the simulated depth of the 20°C isotherm is generally quite good, as is the vertical stratification in the vicinity of the thermocline.

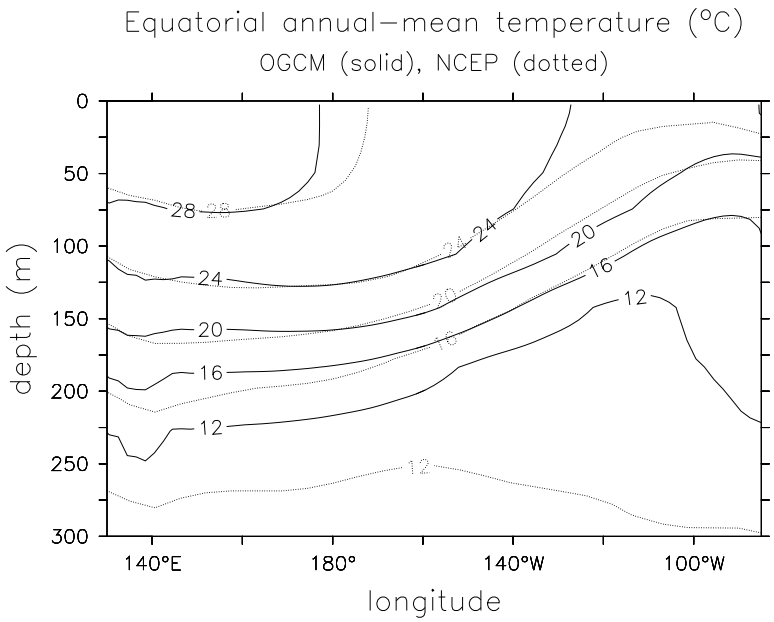

Figure F.3: Vertical section of climatological annual-mean temperature along the equator (2°S–2°N). Solid contours indicate the climatology of the hybrid coupled GCM control run. Dotted contours indicate the 1980–99 climatology from the observational analysis of Behringer et al. (1998).

The annual-mean structure of the equatorial ocean simulated by the model is shown in Fig. F.4. The GCM cold bias at the surface, evident in panel (h), weakens the stratification near the surface in the east (panel d), which promotes vertical mixing. Compared to the NCEP analysis, the GCM has more easterly mixed layer currents in the east, more westerly currents in the west, and stronger upwelling at 50 m depth in the central/eastern Pacific. Note that similar biases in the mixed layer currents were found in the intermediate model (Fig. 4.12). This suggests that either both models are missing some fundamental physics, or that the FSU wind stress forcing is flawed, or that the NCEP ocean analysis is incorrect.

The equatorial heat budget of the top 50 m of the model is shown in Fig. F.5. The equatorial eastern Pacific is cooled primarily through vertical advection. Additional cooling occurs through meridional advection, which peaks around 125°W, and zonal advection, which provides a broad cooling throughout the central basin. Vertical advection is responsible for all of the cooling at the eastern boundary, while zonal advection is responsible for nearly all of the cooling at the dateline. The advective cooling is almost balanced by the surface heat flux, which is into the ocean all along the equator. Adding the advective tendency to the surface flux gives a nonzero residual which is identified with sub-monthly eddies. This eddy flux provides a warming in the east, which is roughly one third as strong as the warming due to surface flux, and a weak cooling in the western Pacific.

Compared to the intermediate model (Fig. 4.14), the GCM has a more active heat budget due to its stronger cold tongue. The cooling due to vertical advection is shifted farther east in the GCM, and the cooling due to zonal advection is zonally broader due to

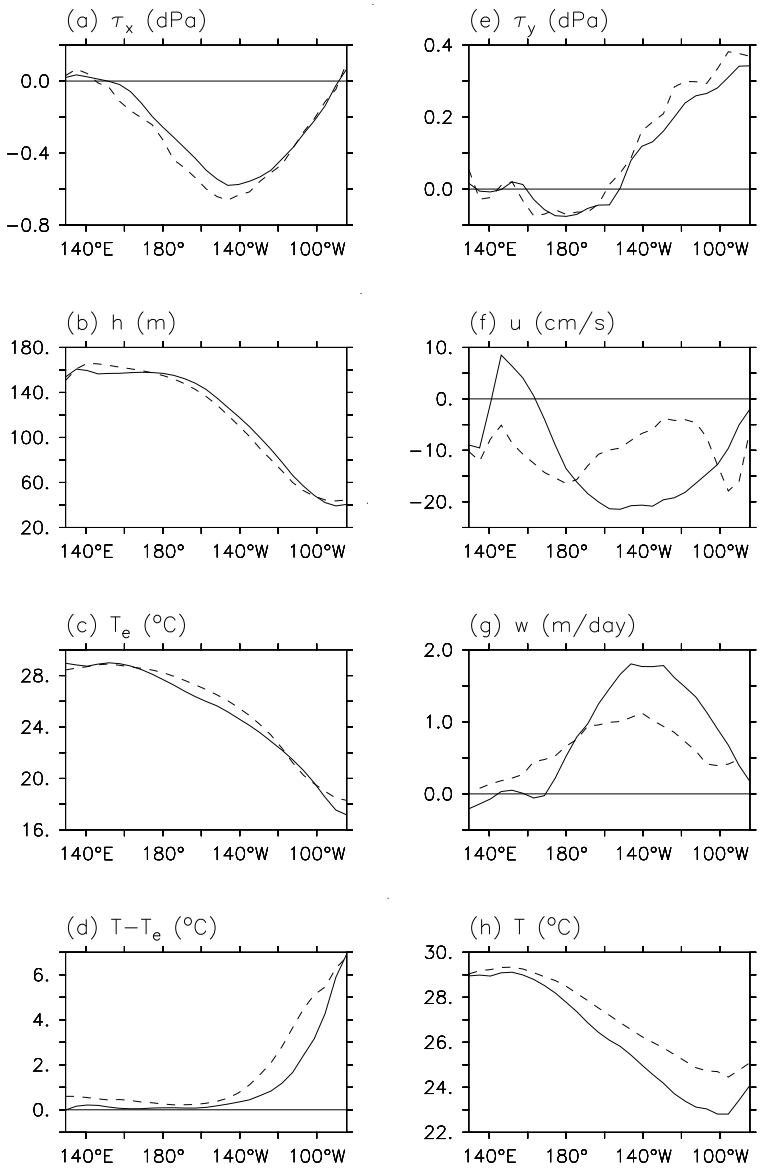

Figure F.4: Annual-mean oceanic climatological fields at the equator (2°S–2°N). Dashed lines are from the observational analysis of Behringer et al. (1998), solid lines are from the control run of the hybrid coupled GCM. (a) Zonal wind stress, (b) depth of the 20° isotherm, (c) temperature at 50 m, (d) temperature at surface minus that at 50 m, (e) meridional wind stress, (f) zonal current averaged over the top 50 m, (g) vertical velocity at 50 m, (h) SST.

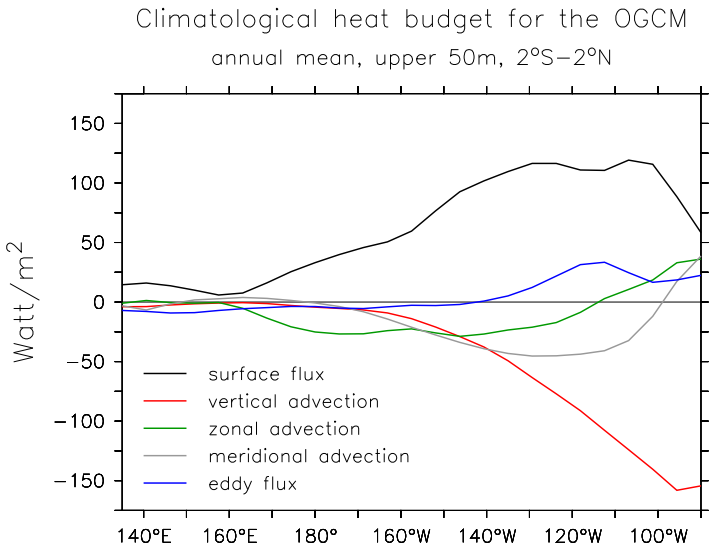

Figure F.5: Annual-mean climatological heat budget of the equatorial band (2°S–2°N), for the top 50 m of the hybrid coupled GCM. Positive values correspond to a warming tendency. Advection and surface fluxes are computed on the full model grid using the total monthly-mean currents and temperatures from the control run, so that effects of the annual cycle and ENSO are included but sub-monthly eddy fluxes are not. The eddy flux tendency is then defined as the heating required to balance the effects of monthly-mean surface flux and advection.

a gentler zonal SST gradient than in the intermediate model. Meridional advection plays rather different roles in these models: in the intermediate ocean, it provides strong cooling at the eastern boundary, while in the GCM, it *warms* the eastern boundary and cools farther west. The eastern boundary warming by meridional advection is a major reason that the GCM also shows a relatively smaller role for surface heat flux in the east.

The GCM eddy fluxes in the east Pacific are largely driven by tropical instability waves (TIWs), which are active in the model as well as in observations (McPhaden et al., 1998; Stockdale et al., 1998; Masina and Philander, 1999a,b; Chelton et al., 2001; Polito et al., 2001; Zhang, 2001). These waves have a period of 20–40 days and so are not well resolved by monthly averages. Comparing Figs. F.5 and 4.14 shows that the amplitude and position of the eddy heat fluxes in the GCM is reasonably well captured by the diffusion term in the intermediate model. Note, however, that the intermediate model assumes a constant diffusivity, i.e. it assumes the eddies have constant amplitude. In reality, TIWs are strongest when the trade winds and cold tongue are strongest, such as during boreal autumn and La Niña. Thus the intermediate model will probably tend to underestimate mixing in the east Pacific during La Niña, and overestimate it during El Niño. The intermediate model also does not capture the small amount of eddy cooling in the central and western Pacific that is evident in the GCM.

Annual cycle

The annual cycle of SST in the model (Fig. F.6) is strongest off-equator and in the vicinity of the cold tongue. Near the coast of South America, SST is warmest in March–April. The annual signal propagates westward along the equator through the calendar year, such that SST peaks in October near the dateline. Associated with these annual variations in SST are seasonal changes in the surface wind stress and currents (not shown), which also propagate westward along the equator. In the central equatorial Pacific, upwelling tends to peak near the end of the calendar year, when the easterly trade winds are at their strongest. The westward equatorial surface currents, on the other hand, are strongest in the central Pacific during August–October and weakest April–June.

F.3.2 Simulated ENSO

Fig. F.7 shows the evolution of the equatorial fields in the hybrid coupled GCM. After four years the model has settled into a self-sustained ENSO with a period of about 3.3 years and a NINO3 SSTA amplitude of about 1.25°C. The oscillation fairly regular, although it is modulated somewhat by the seasonal cycle. Westward propagation of SST anomalies is evident in the central Pacific. Although there is evidence of eastward propagation of the thermocline depth anomalies, the bulk of the thermocline signal in the east is in phase with SSTA in the east. The zonal stress along the equator slightly lags the SSTA in the east, and is more in phase with SSTA in the western Pacific.

The off-equatorial structure of the simulated ENSO cycle is shown in Fig. F.8. The peak SST variability occurs off the coast of Peru, and just south of the equator in the central Pacific. There is westward propagation of SST anomalies almost everywhere in the basin, not just at the equator, and there is a strong poleward spreading of the SST

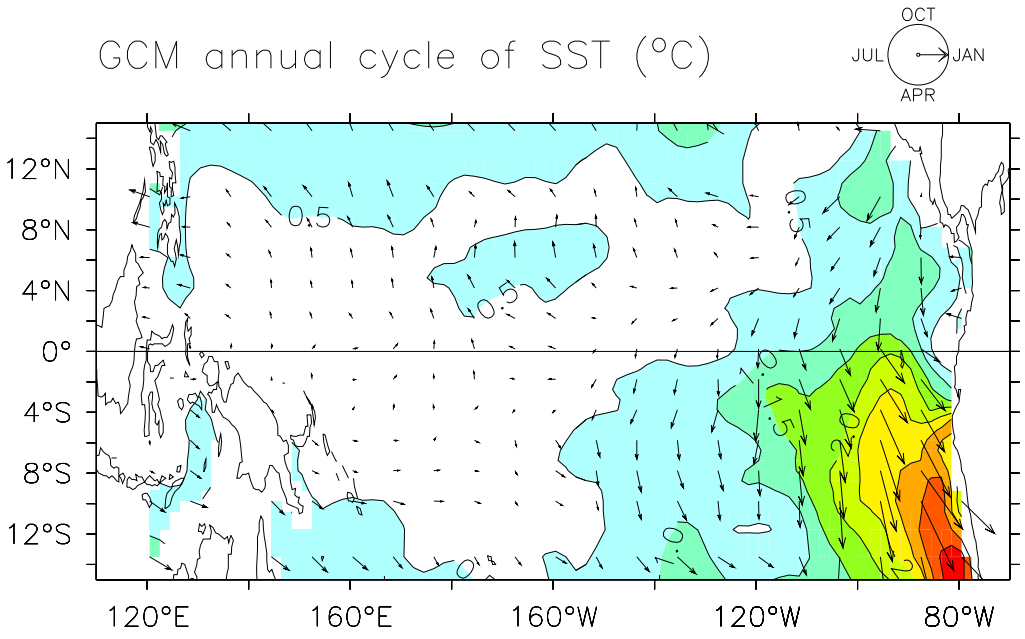

Figure F.6: Annual harmonic of SST from the climatology of the hybrid coupled model. Vectors indicate the month of warmest SST, i.e. rightward-pointing vectors indicate a January peak, downward-pointing vectors an April peak. The vector length corresponds the amplitude of the annual harmonic and is indicated by the contours (°C).

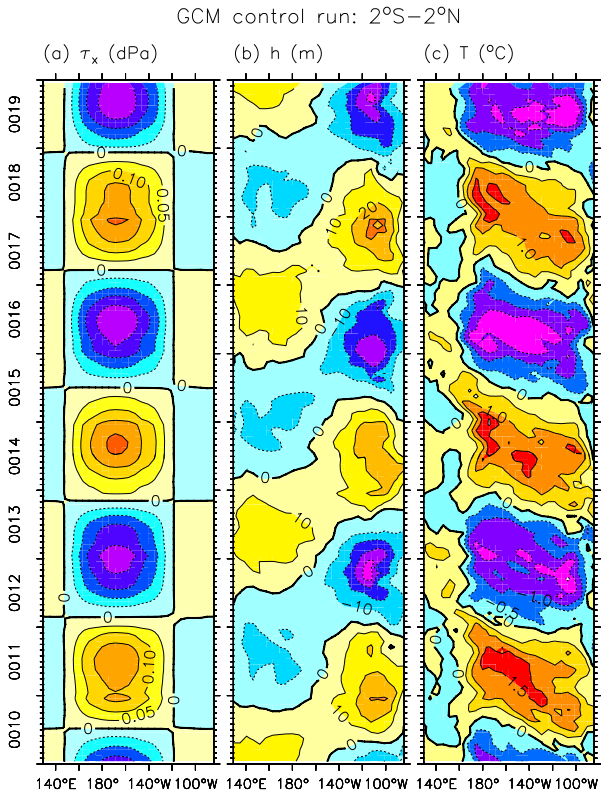

Figure F.7: Representative timeseries of anomaly fields from the hybrid coupled GCM control run, averaged over the equatorial band (2°S–2°N). (a) Zonal stress anomaly (dPa), (b) anomalous depth (m) of the 20°C isotherm, (c) SST anomaly (°C).

anomalies following the equatorial peak.

Fig. F.9 shows the equatorial heat budget for a single ENSO cycle in the GCM. The largest term, $-\overline{w}\partial_z T'$, is active east of 140°W and is a strong amplifier of SSTA in the east. The next largest term is the surface heat flux, which provides a strong damping of SST anomalies across the central and eastern Pacific. The eddy heat fluxes also damp SSTA strongly in the east. The destabilizing effect of $-\overline{w}\partial_z T'$ on the SSTA is enhanced by the meridional advection terms: $-\overline{v}\partial_y T'$ in the eastern basin, and $-v'\partial_y \overline{T}$ in the central basin. All of these terms are nearly in phase or perfectly out of phase with SSTA in the east, and none of these terms shows much sign of zonal propagation.

Enter $-u'\partial_x \overline{T}$, which is active in the central basin and propagates westward at roughly 30 cm s^{-1} (i.e. a 1.7-year basin-crossing time). In the eastern Pacific, this term is nearly in quadrature with SSTA. The $-\overline{u}\partial_x T'$ term is also somewhat in quadrature with SSTA, but no other terms have the amplitude of $-u'\partial_x \overline{T}$ at the crossing points between warm and cold events. Thus $-u'\partial_x \overline{T}$ appears to be an essential oscillation mechanism in the GCM.

The $-w'\partial_z \overline{T}$ term plays a fairly small role except possibly at the far eastern boundary, but even in the east its effect not very coherent with the model ENSO. The nonlinear terms generally small, though they do have rectified effects on the mean state: $-v'\partial_y T'$

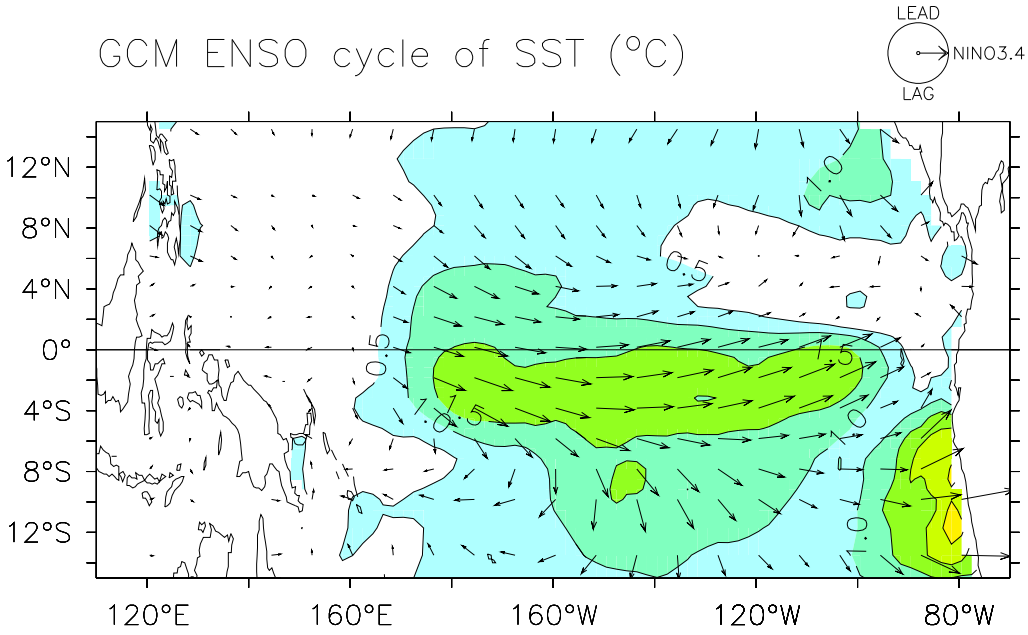

Figure F.8: Amplitude and phase of the ENSO cycle of SST anomalies in the hybrid coupled model. Vectors indicate the SSTA phase relative to the average over the NINO3.4 region (170°W–120°W, 5°S–5°N), i.e. rightward-pointing vectors indicate a peak coincident with NINO3.4 SSTA, downward-pointing vectors a lag of a quarter cycle behind NINO3.4 SSTA. The vector length corresponds the amplitude of the ENSO harmonic and is indicated by the contours (°C). The period of the cycle is 3.3 years.

induces a warming all along the equator, while $-u'\partial_x T'$ and $-w'\partial_z T'$ induce cooling near the dateline and near the eastern boundary, respectively.

There are many similarities between the GCM ENSO and that in the intermediate model control run (Fig. 4.20). In both cases, $-\overline{w}\partial_z T'$ is the dominant destabilizer in the east, surface flux is the primary damping, and $-u'\partial_x \overline{T}$ is a key transitioner in the central Pacific. There are also important differences. Compared to the intermediate model, the GCM shows a greater role for eddy fluxes, which act as an extra damping in the east; the $-\overline{w}\partial_z T'$ term does not lead SSTA as much in the east; and $-\overline{w}\partial_z T'$ does not act as a damping in the central Pacific. The effects of meridional advection are stronger in the GCM, while the effect of $-\overline{u}\partial_x T'$ is weaker.

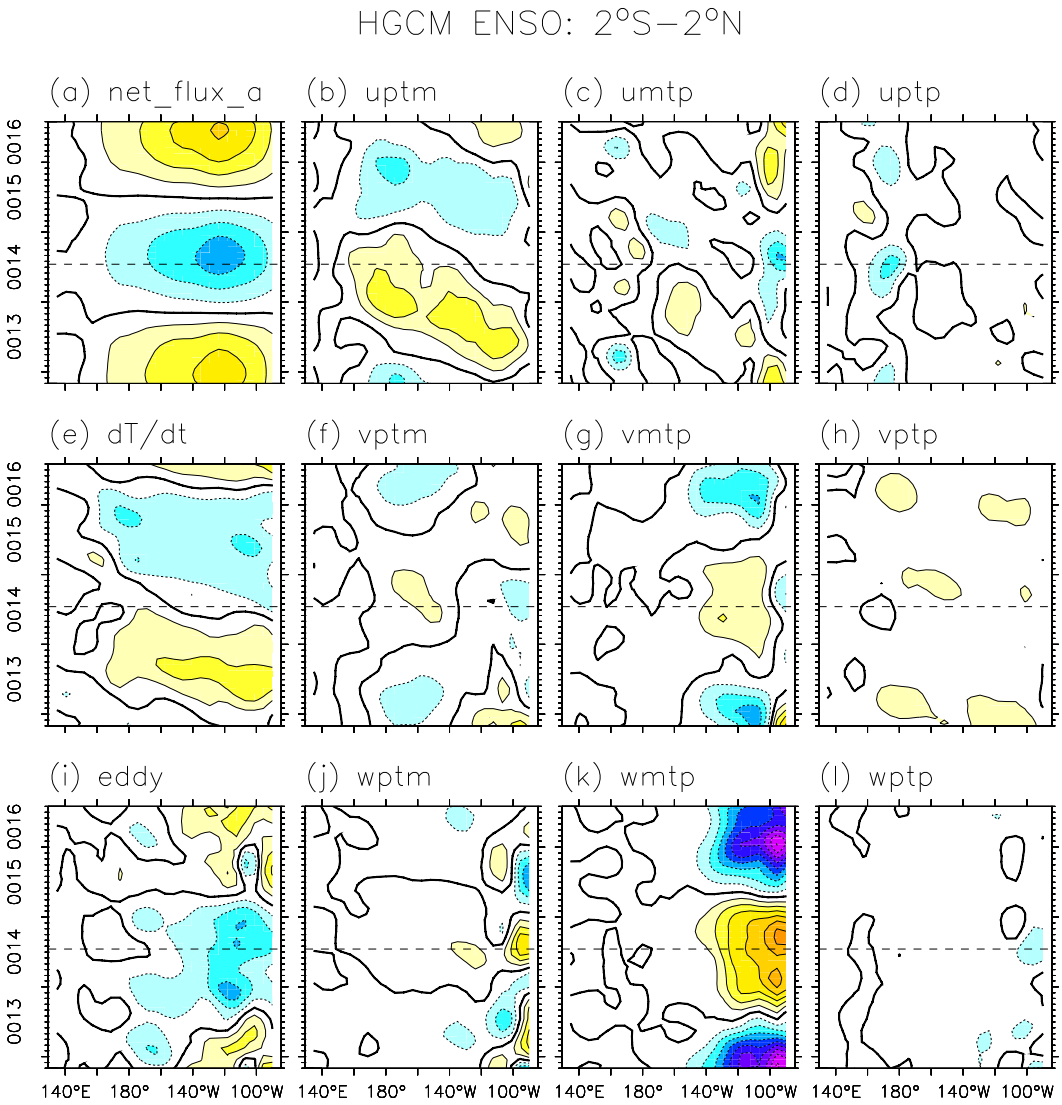

Figure F.9: Temperature anomaly tendency terms for a single ENSO cycle from the hybrid coupled GCM control run, averaged 2°S–2°N and over the upper 50 m of the ocean. Vertical axis indicates years since initialization; dashed line indicates the peak of a warm event. Contour interval is 10 Watts m^{-2}, heavy contour indicates zero; warm colors indicate positive values, cool colors negative values; near-zero values are not shaded. Panels show (a) net heat flux into the ocean, (b) $-u'\partial_x\overline{T}$, (c) $-\overline{u}\partial_x T'$, (d) $-u'\partial_x T'$, (e) $\partial_t T'$, (f) $-v'\partial_y\overline{T}$, (g) $-\overline{v}\partial_y T'$, (h) $-v'\partial_y T'$, (i) eddy flux, (j) $-w'\partial_z\overline{T}$, (k) $-\overline{w}\partial_z T'$, (l) $-w'\partial_z T'$.

Appendix G

Symbols and Definitions

Scalars (real or complex) are indicated by italic Roman or Greek type (u, U, τ_x). Vectors are indicated by bold type ($\mathbf{u}$, $\mathbf{U}$, $\boldsymbol{\tau}$). Matrices are indicated by uppercase bold sans serif type (M).

Diacritical marks

$\overline{\psi}$	time mean of ψ
ψ'	temporal anomaly of ψ: $\psi' \equiv \psi - \overline{\psi}$
ψ^*	rotated coordinates; or perturbation
$\widehat{\psi}$	estimate of ψ from data
$\widetilde{\psi}$	nondimensional ψ; or amplitude of ψ
M'	matrix transpose
M^*	matrix of expansion coefficients (rotated timeseries)
$\widetilde{\mathsf{M}}$	nondimensional matrix

Operators

$\lvert\psi\rvert$	absolute value (magnitude) of ψ: $\lvert\psi\rvert^2 \equiv \mathrm{Re}(\psi)^2 + \mathrm{Im}(\psi)^2$
$\lVert\psi\rVert$	norm of ψ, e.g. the sum of squares of all elements of ψ
$\langle\psi\rangle$	ensemble mean of ψ
curl	vertical component of vector curl
∂_ψ	partial derivative with respect to ψ
$\mathcal{H}\{x(t)\}$	Hilbert transform: $\mathcal{H}\{x(t)\} \equiv \frac{1}{\pi}\int_{-\infty}^{\infty} \frac{x(t')}{t'-t}\,dt'$

$\mathcal{R}(x)$ ramp function: $\mathcal{R}(x) \equiv x\mathcal{S}(x) = \begin{cases} 0 & : \quad x \leq 0 \\ x & : \quad x > 0 \end{cases}$

$\mathcal{R}'(w)$ $\mathcal{R}(w) - \overline{\mathcal{R}(w)}$

$\mathcal{R}^*(w)$ $\mathcal{R}(w) - \mathcal{R}(\overline{w})$

$\mathrm{Re}(\psi)$ real part of ψ

$\mathcal{S}(x)$ Heaviside step function: $\mathcal{S}(x) \equiv \begin{cases} 0 & : \quad x \leq 0 \\ 1 & : \quad x > 0 \end{cases}$

∇^2 horizontal Laplacian operator: $\nabla^2 \equiv \partial_x^2 + \partial_y^2$

Roman symbols (lowercase)

a curvature parameter for T_0

b linear sensitivity of entrainment temperature anomalies to thermocline depth anomalies: $T_e' \approx bh'$

c shallow water gravity wave speed $= (g'H)^{1/2}$

c_d drag coefficient (nondimensional)

e the base of the natural logarithm: $e \equiv \lim_{x \to \infty} \left(1 + \frac{1}{x}\right)^x$

f Coriolis parameter on the equatorial beta plane $= \beta y$; or statistic used in the F-test for variance

g acceleration of gravity at sea level $= 9.81$ m s^{-2}

g' reduced gravity $= g\Delta\rho/\rho$

h thermocline depth anomaly

h_1 linear thermocline depth anomaly

h_m zonal-mean thermocline depth anomaly

h_p zonal-perturbation thermocline depth anomaly: $h_e = h - h_m$

i zonal index; or imaginary unit $(-1)^{1/2}$

j meridional index

k singular value index; or zonal wavenumber

l time index

n number of time points

n_x	total number of longitudinal gridpoints
n_y	total number of latitudinal gridpoints
p	number of SST gridpoints
q	number of wind stress gridpoints
r	dissipation coefficient for active layer mass and momentum; or number of singular values
r_s	damping of active layer shear current (mixed layer viscosity)
s	number of principal components; or sample standard deviation
s_c	sample standard deviation of the climatological ensemble
t	time coordinate
$\mathbf{u}$	average mixed layer current $= (u, v)$
$\mathbf{u}_1$	linear average active layer current
$\mathbf{u_a}$	surface wind $= (u_a, v_a)$
$\mathbf{u}_{al}$	average active layer current
$\mathbf{u}_i$	average active layer current below the mixed layer
$\mathbf{u}_s$	vertical shear current at base of mixed layer $= (u_s, v_s)$
w	upwelling at base of mixed layer
x	zonal coordinate (positive eastward)
x^*	longitude of transient zonal stress patch
x_0	longitude of climatological stress perturbation
x_e	longitude of easternmost gridpoint
x_w	longitude of westernmost gridpoint
y	meridional coordinate (positive northward)
$\tilde{y}$	meridional coordinate nondimensionalized by upwelling scale
y^*	latitude of transient zonal stress patch
y_n	latitude of northernmost gridpoint
y_s	latitude of southernmost gridpoint
z	vertical coordinate (positive upward)

Roman symbols (uppercase)

A	complex coupling factor $A = \|A\| e^{i\theta_A}$, converts SST anomalies to zonal stress anomalies in the simplified equatorial model. The stress anomalies are shifted eastward relative to the SST anomalies by the phase angle θ_A.
B	fraction of the active layer occupied by the unmixed layer: $B \equiv \dfrac{H - H_m}{H}$
F_{ν_1,ν_2}	distribution of a ratio of independent chi-square variables with ν_1 and ν_2 degrees of freedom: $F_{\nu_1,\nu_2} \equiv \dfrac{\chi^2_{\nu_1}/\nu_1}{\chi^2_{\nu_2}/\nu_2}$
H	active layer depth
H_0	active layer depth in the absence of wind stress
H_m	mixed layer depth
H_{obs}	observed active layer depth averaged over the domain of wave propagation
$\mathrm{Im}(\psi)$	imaginary part of ψ
L_e	equatorial radius of deformation $= \left(\dfrac{c}{2\beta}\right)^{1/2} \approx 230$ km $\approx 2.1^\circ$ latitude
L_x	zonal halfwidth of climatological stress perturbation
L_y	meridional halfwidth of climatological stress perturbation
M	number of principal components in the noise model for the residual stress anomalies
N	number of singular modes in the regression model for stress anomalies
N_e	number of ensemble members
$P\{E\}$	probability of event E
PP	predictive power
R_e	reflectivity of the eastern boundary
R_w	reflectivity of the western boundary
T	mixed layer temperature (SST)
$T_0(y)$	equilibrium SST in the absence of ocean dynamics
$T_0(y=0)$	value of T_0 at the equator
T_c	thermocline central temperature

T_e	temperature of water entrained into the mixed layer
T_{min}	minimum temperature in T_e parameterization
$\mathbf{U}$	mixed layer transport $= H_m\mathbf{u}$
$\mathbf{U}_1$	linear total active layer transport $= (U_1, V_1)$
$\mathbf{U}_{1,Kelvin}$	Kelvin component of $\mathbf{U}_1$
$\mathbf{U}_{1,Rossby}$	Rossby component of $\mathbf{U}_1$
$\mathbf{U}_{al}$	total active layer transport $= H\mathbf{u}_{al}$
$\mathbf{U}_i$	active layer transport below the mixed layer $= (H - H_m)\mathbf{u}_{al}$
$\mathbf{U}_s$	shear transport $= H_m\mathbf{u}_s$

Greek symbols (lowercase)

β	variation of Coriolis parameter with latitude at the equator $= 2.28 \times 10^{-11}$ (m s)$^{-1}$ $= 1.97 \times 10^{-6}$ (m day)$^{-1}$ $\approx 2.51 \times 10^{-6}$ (°lat s)$^{-1}$ ≈ 0.217 (°lat day)$^{-1}$
γ	mixed layer entrainment efficiency
δ	temperature increment in T_e parameterization
ϵ	linear damping coefficient for SST
ζ	ratio of time step to noise decorrelation time
κ	horizontal eddy diffusivity in the mixed layer
λ_h	coefficient of thermocline depth
λ_u	coefficient of active layer currents/transport
ϕ_1	lag-1 autocorrelation
ρ	density of seawater
ρ_a	density of surface air
μ	coefficient of wind stress anomalies (coupling strength)
σ^2	variance
σ_c^2	climatological variance
ω	complex frequency in time: $\omega = \omega_r + i\omega_i$
ω_i	angular frequency in time

ω_r	e-folding growth rate in time
$\boldsymbol{\tau}$	vector wind stress on the ocean surface $= (\tau_x, \tau_y)$
τ_x^*	transient zonal stress patch
θ_ψ	phase angle of ψ
$\tilde{\tau}_x^*$	amplitude of transient zonal stress patch
$\overline{\tau}_x^*$	perturbation to climatological zonal stress
$\overline{\tau}_y^*$	perturbation to climatological meridional stress
$\widetilde{\overline{\tau}_x^*}$	amplitude of perturbation to climatological zonal stress
$\widetilde{\overline{\tau}_y^*}$	amplitude of perturbation to climatological meridional stress
χ^2_ν	chi-square variable with ν degrees of freedom

Greek symbols (uppercase)

Δx	grid spacing in zonal direction
Δy	grid spacing in meridional direction
Δx^*	zonal halfwidth of transient zonal stress patch
Δy^*	meridional halfwidth of transient zonal stress patch
Δt	time step
Δt^*	duration of transient zonal stress patch
Γ	maximum $\partial_h T_e$ in T_e parameterization

Matrices

$\mathbf{A}$	dimensionalized left singular vectors of $\mathbf{C}$
$\mathbf{A}_N$	leading N SST singular vectors
$\widetilde{\mathbf{A}}$	left singular vectors of $\mathbf{C}$
$\mathbf{B}$	dimensionalized right singular vectors of $\mathbf{C}$
$\widetilde{\mathbf{B}}$	right singular vectors of $\mathbf{C}$
$\mathbf{B}_{N,\widehat{e}}$	dimensionalized principal component patterns of the residual stress estimated from N singular modes
$\mathbf{B}_{N,\widehat{e},M}$	leading M dimensionalized principal component patterns of the residual stress estimated from N singular modes

$\mathbf{C}$	temporal covariance of observed SST/stress anomalies $= (n-1)^{-1}\mathbf{X}'\mathbf{Y}$
$\mathbf{D}$	diagonal matrix of singular values of $\mathbf{C}$
$\widetilde{\mathbf{D}}$	nondimensionalized diagonal matrix of singular values of $\mathbf{C}$
$\mathbf{E}$	matrix of shocks (spatially-correlated Gaussian noise)
$\mathbf{E}_N$	random shocks plus truncation error
$\widehat{\mathbf{E}}_N$	matrix of residuals (estimate of $\mathbf{E}_N$ from the data)
$\widetilde{\widehat{\mathbf{E}}}^*_{N,\widehat{e}}$	nondimensionalized principal component expansion coefficients of the residual stress estimated using N singular modes
$\mathbf{F}$	red noise model for residual stress principal components
$\mathbf{I}$	identity matrix
$\mathbf{R}_N$	regression of stress anomalies onto the leading N singular vectors of SST
$\widehat{\mathbf{R}}_N$	estimate of $\mathbf{R}_N$ from the data
$\mathbf{S}_{x^*}$	diagonal matrix of SST singular vector expansion coefficient standard deviations
$\mathbf{S}_{y^*}$	diagonal matrix of stress singular vector expansion coefficient standard deviations
$\mathbf{X}$	observed SST anomalies
$\mathbf{X}^*$	singular vector expansion coefficients of SST anomalies
$\widetilde{\mathbf{X}}^*$	nondimensionalized singular vector expansion coefficients of SST anomalies
$\widetilde{\mathbf{X}}^*_N$	leading N nondimensionalized singular vector expansion coefficients of SST anomalies
$\mathbf{Y}$	observed wind stress anomalies
$\mathbf{Y}^*$	singular vector expansion coefficients of stress anomalies
$\widetilde{\mathbf{Y}}^*$	nondimensionalized singular vector expansion coefficients of stress anomalies
$\widehat{\mathbf{Y}}_N$	estimate of deterministic stress anomaly from the leading N singular modes

Appendix H

Units and Conversions

dPa	MKS unit of wind stress = 0.1 Pa = 1 dyne cm^{-2} = 7.46 $\times$ 10^8 kg m^{-1} day^{-2}
cm	centimeter
dyne	CGS unit of force = g cm s^{-2} = 10^{-5} N
°C	Celsius temperature scale, or Celsius degree
km	kilometer
K	Kelvin temperature scale, or Kelvin unit
° lat	degree latitude $\approx$ 1.11 $\times$ 10^5 m at the equator
° lon	degree longitude $\approx$ 1.11 $\times$ 10^5 m at the equator
m	meter
N	Newton (MKS unit of force)
Pa	MKS unit of wind stress = 1 N m^{-2}
s	second
W	Watt (unit of power)
yr	year

Appendix I

Abbreviations and Acronyms

Abbreviations

H_0	null hypothesis
ka	thousand years ago
$NID(\mu, \sigma^2)$	normally and independently distributed with mean μ and variance σ^2
NINO3	eastern equatorial Pacific region (150°W–90°W, 5°S–5°N)
NINO3.4	central equatorial Pacific region (170°W–120°W, 5°S–5°N)
NINO4	western/central equatorial Pacific region (160°E–150°W, 5°S–5°N)
umtp	zonal advection component $-\overline{u}\partial_x T'$
uptm	zonal advection component $-u'\partial_x \overline{T}$
uptp	zonal advection component $-u'\partial_x T'$
vmtp	meridional advection component $-\overline{v}\partial_y T'$
vptm	meridional advection component $-v'\partial_y \overline{T}$
vptp	meridional advection component $-v'\partial_y T'$
wmtp	vertical advection component $-\overline{w}\partial_z T'$
wptm	vertical advection component $-w'\partial_z \overline{T}$
wptp	vertical advection component $-w'\partial_z T'$

Acronyms

AGCM	atmospheric general circulation model
CGS	centimeter-gram-second system of units
CGCM	coupled atmosphere/ocean general circulation model

ENSO	El Niño-Southern Oscillation
EOF	empirical orthogonal function
EWE	easterly wind event
FSU	Florida State University; or the FSU pseudostress analysis
GCM	general circulation model
GFDL	Geophysical Fluid Dynamics Laboratory
HGCM	hybrid coupled general circulation model
ITCZ	Intertropical Convergence Zone
MJO	Madden-Julian Oscillation
MKS	meter-kilogram-second system of units
MOM	Modular Ocean Model
MSD	mean square deviation
NAO	North Atlantic Oscillation
NCAR	The National Center for Atmospheric Research
NCEP	The National Centers for Environmental Prediction; or the NCEP/NCAR reanalysis
OGCM	oceanic general circulation model
OLR	outgoing longwave radiation
PCA	principal components analysis
PDO	Pacific Decadal Oscillation
PP	predictive power
RMS	root mean square
SOI	Southern Oscillation Index (surface air pressure at Tahiti minus that at Darwin, Australia)
SPCZ	South Pacific Convergence Zone
SSE	sum of square errors
SST	sea surface temperature
SSTA	sea surface temperature anomaly

SVD	singular value decomposition
TIW	tropical instability wave
UNESCO	United Nations Educational, Scientific, and Cultural Organization
WWE	westerly wind event

Bibliography

AchutaRao, K. and K. R. Sperber, 2002: Simulation of the El Niño Southern Oscillation: Results from the Coupled Model Intercomparison Project. *Climate Dyn.*, **19**, 191–209. 4, 7, 8, 9, 145

AMS Council, 2001: Statement on seasonal to interannual climate prediction. *Bull. Amer. Meteor. Soc.*, **82**, 701–710. 2

An, S.-I. and F.-F. Jin, 2000: An eigen analysis of the interdecadal changes in the structure and frequency of ENSO mode. *Geophys. Res. Lett.*, **27**, 2573–2576. 13, 177, 180

An, S.-I. and F.-F. Jin, 2001: Collective role of thermocline and zonal advective feedbacks in the ENSO mode. *J. Climate*, **14**, 3421–3432. 149, 177, 178, 186

An, S.-I. and I.-S. Kang, 2000: A further investigation of the recharge oscillator paradigm for ENSO using a simple coupled model with the zonal mean and eddy separated. *J. Climate*, **13**, 1987–1993. 92, 93, 185

An, S.-I. and B. Wang, 2000: Interdecadal change of the structure of the ENSO mode and its impact on the ENSO frequency. *J. Climate*, **13**, 2044–2055. 13, 22, 26, 38, 45, 56, 149

Anderson, D. L. T., E. S. Sarachik, P. J. Webster, and L. M. Rothstein, 1998: The TOGA Decade: Reviewing the progress of El Niño research and prediction. *J. Geophys. Res.*, **103**, 14 167–14 510. 2

Andreasen, D. H., A. C. Ravelo, and A. J. Broccoli, 2001: Remote forcing at the last glacial maximum in the tropical Pacific ocean. *J. Geophys. Res.*, **106**, 879–897. 15

Auad, G., J. Miller, J. O. Roads, and D. Cayan, 2001: Pacific ocean wind stress and surface heat flux anomalies from NCEP reanalysis and observations: Cross-statistics and ocean model responses. *J. Geophys. Res.*, **106**, 22 249–22 265. 24, 99

Balmaseda, M. A., D. L. T. Anderson, and M. K. Davey, 1994: ENSO prediction using a dynamical ocean model coupled to statistical atmospheres. *Tellus*, **46A**, 497–511. 56

Balmaseda, M. A., M. K. Davey, and D. L. T. Anderson, 1995: Decadal and seasonal dependence of ENSO prediction skill. *J. Climate*, **8**, 2705–2715. 132

Barnett, T. P., G. Hegerl, T. Knutson, and S. Tett, 2000: Uncertainty levels in predicted patterns of anthropogenic climate change. *J. Geophys. Res.*, **105**, 15 525–15 542. 16

Barnett, T. P., M. Latif, N. Graham, M. Flügel, S. Pazan, and W. White, 1993: ENSO and ENSO-related predictability. Part I: Prediction of equatorial sea surface temperature with a hybrid coupled ocean-atmosphere model. *J. Climate*, **6**, 1545–1566. 56

Barnett, T. P., M. Latif, E. Kirk, and E. Roeckner, 1991: On ENSO physics. *J. Climate*, **4**, 487–515. 99

Barnett, T. P., D. W. Pierce, M. Latif, D. Dommenget, and R. Saravanan, 1999: Interdecadal interactions between the tropics and midlatitudes in the Pacific basin. *Geophys. Res. Lett.*, **26**, 615–618. 12, 13

Barnston, A. G., 1995: Our improving capability in ENSO forecasting. *Weather*, **50**, 419. 132

Barnston, A. G., M. H. Glantz, and Y. He, 1999a: Predictive skill of statistical and dynamical climate models in SST forecasts during the 1997–98 El Niño episode and the 1998 La Niña onset. *Bull. Amer. Meteor. Soc.*, **80**, 217–243. 4

Barnston, A. G., A. Leetmaa, V. E. Kousky, R. E. Livezey, E. A. O' Lenic, H. M. van den Dool, A. J. Wagner, and D. A. Unger, 1999b: NCEP forecasts of the El Niño of 1997–98 and its U.S. impacts. *Bull. Amer. Meteor. Soc.*, **80**, 1829–1852. 4

Barnston, A. G., et al., 1994: Long-lead seasonal forecasts—Where do we stand? *Bull. Amer. Meteor. Soc.*, **75**, 2097–2114. 2

Battisti, D. S., 1988: Dynamics and thermodynamics of a warming event in a coupled tropical atmosphere-ocean model. *J. Atmos. Sci.*, **45**, 2889–2919. 86, 92, 93, 132, 144

Battisti, D. S., 1989: On the role of off-equatorial oceanic Rossby waves during ENSO. *J. Phys. Oceanogr.*, **19**, 551–559. 200

Battisti, D. S. and A. C. Hirst, 1989: Interannual variability in a tropical atmosphere-ocean model: Influence of the basic state, ocean geometry and nonlinearity. *J. Atmos. Sci.*, **46**, 1687–1712. 18, 123, 175, 178, 179, 180

Battisti, D. S. and E. S. Sarachik, 1995: Understanding and predicting ENSO. *Rev. Geophys.*, **July 1995 Suppl.**, 1367–1376. 132

Battisti, D. S., E. S. Sarachik, and A. C. Hirst, 1999: A consistent model for the large-scale steady surface atmospheric circulation in the tropics. *J. Climate*, **12**, 2956–2964. 40

Behringer, D. W., M. Ji, and A. Leetmaa, 1998: An improved coupled model for ENSO prediction and implications for ocean initialization. Part I: The ocean data assimilation system. *Mon. Wea. Rev.*, **126**, 1013–1021. 26, 85, 92, 94, 95, 96, 97, 98, 100, 102, 103, 104, 107, 108, 266, 267

Blanke, B., J. D. Neelin, and D. Gutzler, 1997: Estimating the effect of stochastic wind stress forcing on ENSO irregularity. *J. Climate*, **10**, 1473–1486. 56, 129, 253

Boer, G. J., G. Flato, and D. Ramsden, 2000: A transient climate change simulation with greenhouse gas and aerosol forcing: Projected climate to the twenty-first century. *Climate Dyn.*, **16**, 427–450. 16, 17

Bonekamp, H., G. J. van Oldenborgh, and G. Burgers, 2001: Variational assimilation of tropical atmosphere-ocean and expendable bathythermograph data in the Hamburg Ocean Primitive Equation ocean general circulation model, adjusting the surface fluxes in the tropical ocean. *J. Geophys. Res.*, **106**, 16 693–16 709. 23

Bony, S., K.-M. Lau, and Y. C. Sud, 1997: Sea surface temperature and large-scale circulation influences on tropical greenhouse effect and cloud radiative forcing. *J. Climate*, **10**, 2055–2077. 17

Boulanger, J.-P. and C. Menkes, 1999: Long equatorial wave reflection in the Pacific ocean from TOPEX/POSEIDON data during the 1992–1998 period. *Climate Dyn.*, **15**, 205–225. 86, 93

Bretherton, C. S., C. Smith, and J. M. Wallace, 1992: An intercomparison of methods for finding coupled patterns in climate data. *J. Climate*, **5**, 541–560. 58

Busalacchi, A. J., R. M. Atlas, and E. C. Hackert, 1993: Comparison of Special Sensor Microwave Imager vector wind stress with model-derived and subjective products for the tropical Pacific. *J. Geophys. Res.*, **98**, 6961–6977. 24

Busalacchi, A. J. and M. A. Cane, 1988: The effect of varying stratification on low-frequency equatorial motions. *J. Phys. Oceanogr.*, **18**, 801–812. 178

Busalacchi, A. J. and J. J. O'Brien, 1981: Interannual variability of the equatorial Pacific in the 1960's. *J. Geophys. Res.*, **86**, 10 901–10 907. 91

Bush, A. B. G., 1999: Assessing the impact of mid-Holocene insolation on the atmosphere-ocean system. *Geophys. Res. Lett.*, **26**, 99–102. 14

Bush, A. B. G. and S. G. H. Philander, 1998: The role of ocean-atmosphere interactions in tropical cooling during the last glacial maximum. *Science*, **279**, 1341–1344. 15

Cane, M. A., 1984: Modeling sea level during El Niño. *J. Phys. Oceanogr.*, **14**, 1864–1874. 92

Cane, M. A., 1992: Comments on "The fast-wave limit and interannual oscillations". *J. Atmos. Sci.*, **49**, 1947–1949. 187

Cane, M. A., A. C. Clement, A. Kaplan, Y. Kushnir, D. Pozdnyakov, R. Seager, S. E. Zebiak, and R. Murtugudde, 1997: Twentieth century sea surface temperature trends. *Science*, **275**, 957–960. 16, 161, 169

Cane, M. A. and P. Molnar, 2001: Closing of the Indonesian seaway as a precursor to east African aridification around 3–4 million years ago. *Nature*, **411**, 157–162. 15

Cane, M. A. and R. J. Patton, 1984: A numerical model for low-frequency equatorial dynamics. *J. Phys. Oceanogr.*, **14**, 1853–1863. 89

Cane, M. A. and E. S. Sarachik, 1976: Forced baroclinic ocean motions: I. The linear equatorial unbounded case. *J. Mar. Res.*, **34**, 629–665. 139

Cane, M. A. and E. S. Sarachik, 1977: Forced baroclinic ocean motions: II. The linear equatorial bounded case. *J. Mar. Res.*, **35**, 395–432. 86, 139, 163

Cane, M. A. and E. S. Sarachik, 1979: Forced baroclinic ocean motions: III. The linear equatorial basin case. *J. Mar. Res.*, **37**, 355–398. 139

Cane, M. A., S. E. Zebiak, and S. C. Dolan, 1986: Experimental forecasts of El Niño. *Nature*, **321**, 827–832. 3

Cane, M. A., S. E. Zebiak, and Y. Xue, 1995: Model studies of the long-term behavior of ENSO. *Natural Climate Variability on Decade-to-Century Time Scales*, National Academy Press, 442–457. 14

Cardone, V. J., J. G. Greenwood, and M. A. Cane, 1990: On trends in historical marine wind data. *J. Climate*, **3**, 113–127. 22

Casey, K. S. and P. Cornillon, 2001: Global and regional sea surface temperature trends. *J. Climate*, **14**, 3801–3818. 10

Cassou, C. and C. Perigaud, 2000: ENSO simulated with intermediate coupled models and evaluated with observations over 1970–1998. Part II: Role of the off-equatorial ocean and meridional winds. *J. Climate*, **13**, 1635–1663. 22, 38, 40, 56, 91, 253

Cayan, D. R., 1992: Latent and sensible heat flux anomalies over the northern oceans: Driving the sea surface temperature. *J. Phys. Oceanogr.*, **22**, 859–881. 99

Cess, R. D., G. L. Potter, and Coauthors, 1989: Interpretation of cloud-climate feedback as produced by 14 atmospheric general circulation models. *Science*, **245**, 513–516. 17

Cess, R. D., G. L. Potter, and Coauthors, 1990: Intercomparison and interpretation of climate feedback processes in 19 atmospheric general circulation models. *J. Geophys. Res.*, **95**, 16 601–16 615. 17

Chang, P., 1994: A study of the seasonal cycle of sea surface temperature in the tropical Pacific Ocean using reduced gravity models. *J. Geophys. Res.*, **99**, 7725–7741. 91, 188

Chang, P., L. Ji, H. Li, and M. Flügel, 1996: Chaotic dynamics versus stochastic processes in El Niño-Southern Oscillation in coupled ocean-atmosphere models. *Physica D*, **98**, 301–320. 19, 129

Chang, P. and S. G. H. Philander, 1994: A coupled ocean-atmosphere instability of relevance to the seasonal cycle. *J. Atmos. Sci.*, **51**, 3627–3648. 149, 188

Chao, Y., M. Ghil, and J. C. McWilliams, 2000: Pacific interdecadal variability in this century's sea surface temperatures. *Geophys. Res. Lett.*, **27**, 2261–2264. 10, 12

Chelton, D. B., et al., 2001: Observations of coupling between surface wind stress and sea surface temperature in the eastern tropical Pacific. *J. Climate*, **14**, 1479–1498. 269

Chen, D., M. A. Cane, and S. E. Zebiak, 1999: The impact of NSCAT winds on predicting the 1997/1998 El Niño: A case study with the Lamont-Doherty Earth Observatory model. *J. Geophys. Res.*, **104**, 11 321–11 327. 24, 85

Chen, D., S. E. Zebiak, A. J. Busalacchi, and M. A. Cane, 1995: An improved procedure for El Niño forecasting: Implications for predictability. *Science*, **269**, 1699–1702. 25, 132

Chen, J., B. E. Carlson, and A. D. Del Genio, 2002: Evidence for strengthening of the tropical general circulation in the 1990s. *Science*, **295**, 838–841. 12

Cherry, S., 1996: Singular value decomposition analysis and canonical correlation analysis. *J. Climate*, **9**, 2003–2009. 58

Cherry, S., 1997: Some comments on singular value decomposition analysis. *J. Climate*, **10**, 1759–1761. 58

Clarke, A. J., 1991: On the reflection and transmission of low-frequency energy at the irregular Western Pacific Ocean boundary. *J. Geophys. Res.*, **96**, 3289–3305. 86, 93

Clarke, A. J. and A. Lebedev, 1996: Long-term changes in the equatorial Pacific trade winds. *J. Climate*, **9**, 1020–1029. 10, 23

Clarke, A. J. and A. Lebedev, 1997: Interannual and decadal changes in equatorial wind stress in the Atlantic, Indian, and Pacific oceans and the eastern ocean coastal response. *J. Climate*, **10**, 1722–1729. 10, 22, 23

Clement, A. C., M. A. Cane, and R. Seager, 2001: An orbitally driven tropical source for abrupt climate change. *J. Climate*, **14**, 2369–2375. 15

Clement, A. C., R. Seager, and M. A. Cane, 1999: Orbital controls on the El Niño/Southern Oscillation and the tropical climate. *Paleoceanogr.*, **14**, 441–456. 15

Clement, A. C., R. Seager, M. A. Cane, and S. E. Zebiak, 1996: An ocean dynamical thermostat. *J. Climate*, **9**, 2190–2196. 16, 17, 161, 169

Codron, F., 2001: Sensitivity of the tropical Pacific to a change of orbital forcing in two versions of a coupled GCM. *Climate Dyn.*, **17**, 187–203. 14

Codron, F., A. Vintzileos, and R. Sadourny, 2001: Influence of mean state changes on the structure of ENSO in a tropical coupled GCM. *J. Climate*, **14**, 730–742. 18, 181

Cole, J., 2001: A slow dance for El Niño. *Science*, **291**, 1496–1497. 14, 15

Colinvaux, P., 1972: Climate and the Galápagos Islands. *Nature*, **240**, 17–20. 14

Collins, M., 2000a: The El Niño-Southern Oscillation in the Second Hadley Centre Coupled Model and its response to greenhouse warming. *J. Climate*, **13**, 1299–1312. 17

Collins, M., 2000b: Understanding uncertainties in the response of ENSO to greenhouse warming. *Geophys. Res. Lett.*, **27**, 3509–3512. 17

Curtis, S. and S. Hastenrath, 1999: Long-term trends and forcing mechanisms of circulation and climate in the equatorial Pacific. *J. Climate*, **12**, 1134–1144. 10

da Silva, A. M., C. C. Young, and S. Levitus, 1994: Atlas of Surface Marine Data 1994, Vol. 1: Algorithms and Procedures. NOAA Atlas NESDIS 6, U.S. Department of Commerce, 83 pp., Washington, D.C. 22, 23, 26

D'Agostino, R. B. and M. A. Stephens, (Eds.) , 1986: *Goodness-of-fit techniques*. Dekker, New York, 560pp. 49

Dai, A., T. M. L. Wigley, B. A. Boville, J. T. Kiehl, and L. E. Buja, 2001: Climates of the twentieth and twenty-first centuries simulated by the NCAR Climate System Model. *J. Climate*, **14**, 485–519. 16, 145

D'Arrigo, R., R. Villalba, and G. Wiles, 2001: Tree-ring estimates of Pacific decadal climate variability. *Climate Dyn.*, **18**, 219–224. 12

Davey, M. K., M. Huddleston, K. R. Sperber, and model data contributors, 2000: STOIC: A study of coupled GCM climatology and variability in tropical ocean regions. STOIC project report, CLIVAR-WGSIP, 41 pp. 6

Davey, M. K., M. Huddleston, K. R. Sperber, and model data contributors, 2002: STOIC: A study of coupled model climatology and variability in tropical ocean regions. *Climate Dyn.*, **18**, 403–420. 4, 6, 8

Delcroix, T., 1998: Observed surface oceanic and atmospheric variability in the tropical Pacific at seasonal and ENSO timescales: A tentative overview. *J. Geophys. Res.*, **103**, 18 611–18 633. 188

Delecluse, P., M. K. Davey, Y. Kitamura, S. G. H. Philander, M. Suarez, and L. Bengtsson, 1998: Coupled general circulation modeling of the tropical Pacific. *J. Geophys. Res.*, **103**, 14 357–14 373. 3, 145, 188

DeVries, T. J., L. Ortlieb, A. Diaz, L. Wells, and C. Hillaire-Marcel, 1997: Determining the early history of El Niño. *Science*, **276**, 965–966. 14

DeWitt, D. G. and E. K. Schneider, 1998: The tropical ocean response to a change in orbital forcing. Technical Report 56, COLA. 14

Dewitte, B., 2000: Sensitivity of an intermediate ocean-atmosphere coupled model of the tropical Pacific to its oceanic vertical structure. *J. Climate*, **13**, 2363–2388. 178

Dewitte, B. and C. Perigaud, 1996: El Niño-La Niña events simulated with Cane and Zebiak's model and observed with satellite or in situ data. Part II: Model forced with observations. *J. Climate*, **9**, 1188–1207. 25, 91

Diaz, H. F. and R. S. Pulwarty, 1994: An analysis of the time scales of variability in centuries-long ENSO-sensitive records in the last 1000 years. *Climatic Change*, **26**, 317–342. 14

Dijkstra, H. A. and J. D. Neelin, 1995: Ocean-atmosphere interaction and the tropical climatology. Part II: Why the Pacific cold tongue is in the east. *J. Climate*, **8**, 1343–1359. 28, 138, 145, 150, 153, 161, 179

Dijkstra, H. A. and J. D. Neelin, 1999: Coupled processes and the tropical climatology. Part III: Instabilities of the fully coupled climatology. *J. Climate*, **12**, 1630–1643. 18, 175, 179

du Penhoat, Y. and M. A. Cane, 1991: Effect of low-latitude western boundary gaps on the reflection of equatorial motions. *J. Geophys. Res.*, **96**, 3307–3322. 93

Dunbar, R. B., G. M. Wellington, M. W. Colgan, and P. W. Glynn, 1994: Eastern Pacific sea surface temperature since 1600 A.D.: The δ^{18}O record of climate variability in Galápagos corals. *Paleoceanogr.*, **9**, 291–315. 12, 14

Dutton, J. F., C. J. Poulsen, and J. L. Evans, 2000: The effect of global climate change on the regions of tropical convection in CSM1. *Geophys. Res. Lett.*, **27**, 3049–3052. 17

Easterling, D. R., G. A. Meehl, C. Parmesan, S. A. Chagnon, T. R. Karl, and L. O. Mearns, 2000: Climate extremes: Observations, modeling, and impacts. *Science*, **289**, 2068–2074. 17

Eckert, C. and M. Latif, 1997: Predictability of a stochastically forced hybrid coupled model of El Niño. *J. Climate*, **10**, 1488–1504. 56, 131

Enfield, D. B., 2001: Evolution and historical perspective of the 1997–1998 El Niño-Southern Oscillation event. *Bull. Marine Sci.*, **63**, 7–25. 5

Enfield, D. B. and L. Cid, 1991: Low-frequency changes in El Niño-Southern Oscillation. *J. Climate*, **4**, 1137–1146. 13

Enfield, D. B. and A. M. Mestas-Nuñez, 1999: Interannual-to-multidecadal climate variability and its relationship to global sea surface temperatures. *Inter-Hemispheric Climate Linkages*, V. Markgraf, Ed., Academic Press, 17–29. 12, 14

Esbensen, S. and V. Kushnir, 1981: The heat budget of the global ocean — an atlas based on estimates from surface marine observations. Technical Report 29, Clim. Res. Inst., Oregon State Univ., Corvallis, OR. 263

Farrell, J., T. Pedersen, S. Calvert, and B. Nielsen, 1995: Glacial-interglacial changes in the equatorial Pacific ocean. *Nature*, **377**, 514–517. 14

Fedorov, A. V., 2002: The response of the coupled tropical ocean-atmosphere to westerly wind bursts. *Quart. J. Roy. Meteor. Soc.*, **128**, 1–23. 18, 181

Fedorov, A. V. and S. G. Philander, 2000: Is El Niño changing? *Science*, **288**, 1997–2002. 18, 149, 181

Fedorov, A. V. and S. G. Philander, 2001: A stability analysis of tropical ocean-atmosphere interactions: Bridging measurements and theory for El Niño. *J. Climate*, **14**, 3086–3101. 18, 181

Flügel, M. and P. Chang, 1996: Impact of dynamical and stochastic processes on the predictability of ENSO. *Geophys. Res. Lett.*, **23**, 2089–2092. 129

Flügel, M. and P. Chang, 1998: Does the predictability of ENSO depend on the seasonal cycle? *J. Atmos. Sci.*, **55**, 3230–3243. 132

Fu, R., A. D. Del Genio, W. B. Rossow, and W. T. Liu, 1992: Cirrus-cloud thermostat for tropical sea surface temperatures tested using satellite data. *Nature*, **358**, 394–397. 16

Gagan, M. K., L. K. Ayliffe, D. Hopley, J. A. Cali, G. E. Mortimer, J. Chappell, M. T. McCulloch, and M. J. Head, 1998: Temperature and surface-ocean water balance of the mid-Holocene tropical western Pacific. *Science*, **279**, 1014–1017. 14

Galanti, E. and E. Tziperman, 2000: ENSO's phase locking to the seasonal cycle in the fast-SST, fast-wave, and mixed mode regimes. *J. Atmos. Sci.*, **57**, 2936–2950. 28

Gibson, J., P. Kållberg, S. Uppala, A. Nomura, A. Hernandez, and E. Serrano, 1997: ECMWF Reanalysis Project Report Series. Technical Report 1, ECMWF, Shinfield Park, Reading, United Kingdom. 265

Giese, B. S. and J. A. Carton, 1999: Interannual and decadal variability in the tropical and midlatitude Pacific ocean. *J. Climate*, **12**, 3402–3418. 12

Giese, B. S., S. C. Urizar, and N. S. Fuckar, 2002: Southern hemisphere origins of the 1976 climate shift. *Geophys. Res. Lett.*, **29**, doi:10.1029/2001GL013268. 12

Gill, A. E., 1980: Some simple solutions for heat-induced tropical circulation. *Quart. J. Roy. Meteor. Soc.*, **106**, 447–462. 23

Gill, A. E., 1982: *Atmosphere-Ocean Dynamics*. Academic Press, San Diego, 662pp. 139

Goddard, L., S. J. Mason, S. E. Zebiak, C. F. Ropelewski, R. Basher, and M. A. Cane, 2001: Current approaches to seasonal to interannual climate predictions. *Int. J. Climatol.*, **21**, 1111–1152. 2

Goddard, L. and S. G. Philander, 2000: The energetics of El Niño and La Niña. *J. Climate*, **13**, 1496–1516. 116

Gordon, C. T., A. Rosati, and R. Gudgel, 2000: Tropical sensitivity of a coupled model to specified ISCCP low clouds. *J. Climate*, **13**, 2239–2260. 181

Goswami, B. N. and J. Shukla, 1991: Predictability of a coupled ocean-atmosphere model. *J. Climate*, **4**, 3–22. 131, 132

Goswami, B. N. and M. A. Thomas, 2000: Coupled ocean-atmosphere inter-decadal modes in the tropics. *J. Meteor. Soc. Japan*, **78**, 765–775. 12

Graham, N. E., 1994: Decadal-scale climate variability in the tropical and North Pacific during the 1970s and 1980s: Observations and model results. *Climate Dyn.*, **10**, 135–162. 12, 24, 34, 45

Grodsky, S. A. and J. A. Carton, 2001: Intense surface currents in the tropical Pacific during 1996–1998. *J. Geophys. Res.*, **106**, 16 673–16 684. 93

Gu, D. and S. G. H. Philander, 1995: Secular changes of annual and interannual variability in the tropics during the past century. *J. Climate*, **8**, 864–876. 3, 13, 45

Gu, D. and S. G. H. Philander, 1997: Interdecadal climate fluctuations that depend on exchanges between the tropics and extratropics. *Science*, **275**, 805–807. 12, 16, 150

Gudgel, R. G., A. Rosati, and C. T. Gordon, 2001: The sensitivity of a coupled atmospheric-oceanic GCM to prescribed low-level clouds over the ocean and tropical landmasses. *Mon. Wea. Rev.*, **129**, 2103–2115. 138

Gutzler, D. S., 1993: Modes of large-scale ocean-atmosphere interaction in the tropical Pacific. *Proc. 17th Annual NOAA Climate Diagnostics Workshop*, Norman, OK, Natl. Ocean. Atmos. Admin., 77–80, nTIS PB93–183895. 61

Hao, Z., J. D. Neelin, and F.-F. Jin, 1993: Nonlinear tropical air-sea interaction in the fast-wave limit. *J. Climate*, **6**, 1523–1544. 18, 149, 175, 177, 181

Harrison, D. E., W. S. Kessler, and B. S. Giese, 1989: Ocean circulation model hindcasts of the 1982–83 El Niño: Thermal variability along the ship-of-opportunity tracks. *J. Phys. Oceanogr.*, **19**, 397–418. 22, 24

Harrison, D. E. and N. K. Larkin, 1997: Darwin sea level pressure, 1876–1996: evidence for climate change? *Geophys. Res. Lett.*, **24**, 1779–1782. 10, 14

Harrison, D. E. and N. K. Larkin, 1998: ENSO sea surface temperature and wind anomalies, 1946–1993. *Rev. Geophys.*, **36**, 353–399. 3, 26, 66

Harrison, M. J., A. Rosati, B. J. Soden, E. Galanti, and E. Tziperman, 2002: An evaluation of air-sea flux products for ENSO simulation and prediction. *Mon. Wea. Rev.*, **130**, 723–732. 24, 56, 263, 265

Hartmann, D. L., 2002: Tropical surprises. *Science*, **295**, 811–812. 12

Hartmann, D. L. and M. L. Michelson, 1993: Large-scale effects on the regulation of tropical sea surface temperature. *J. Climate*, **6**, 2049–2062. 16

Hayashi, Y., 1986: Statistical interpretations of ensemble-time mean predictability. *J. Meteor. Soc. Japan*, **64**, 167–181. 132

Hazeleger, W., M. Visbeck, M. Cane, A. Karspeck, and N. Naik, 2001: Decadal upper ocean temperature variability in the tropical Pacific. *J. Geophys. Res.*, **106**, 8971–8988. 13

Hellerman, S. and M. Rosenstein, 1983: Normal monthly wind stress over the world ocean with error estimates. *J. Phys. Oceanogr.*, **13**, 1093–1104. 24, 263

Hirst, A. C., 1985: Free equatorial instabilities in simple coupled atmosphere-ocean models. *Coupled Ocean-Atmosphere Models*, J. C. J. Nihoul, Ed., Elsevier, Amsterdam, 153–165. 177

Hirst, A. C., 1986: Unstable and damped equatorial modes in simple coupled ocean-atmosphere models. *J. Atmos. Sci.*, **43**, 606–630. 18, 175, 177

Hirst, A. C., 1988: Slow instabilities in tropical ocean basin-global atmosphere models. *J. Atmos. Sci.*, **45**, 830–852. 177, 179

Houtekamer, P. L., 1995: The construction of optimal perturbations. *Mon. Wea. Rev.*, **123**, 2181–2196. 81

Hu, Z.-Z., L. Bengtsson, E. Roeckner, M. Christoph, A. Bacher, and J. M. Oberhuber, 2001: Impact of global warming on the interannual and interdecadal climate modes in a coupled GCM. *Climate Dyn.*, **17**, 361–374. 17

Huang, B. and Z. Liu, 2001: Temperature trend of the last 40 yr in the upper Pacific ocean. *J. Climate*, **14**, 3738–3750. 10, 17

Huang, R. X. and J. Pedlosky, 2000: Climate variability of the equatorial thermocline inferred from a two-moving-layer model of the ventilated thermocline. *J. Phys. Oceanogr.*, **30**, 2610–2626. 12

Hughen, K. A., D. P. Schrag, S. B. Jacobsen, and W. Hantoro, 1999: El Niño during the last interglacial period recorded by a fossil coral from Indonesia. *Geophys. Res. Lett.*, **26**, 3129–3132. 15

Ji, M., D. W. Behringer, and A. Leetmaa, 1998: An improved coupled model for ENSO prediction and implications for ocean initialization. Part II: The coupled model. *Mon. Wea. Rev.*, **126**, 1022–1034. 26

Jin, F.-F., 1996: Tropical ocean-atmosphere interaction, the Pacific cold tongue, and the El Niño-Southern Oscillation. *Science*, **274**, 76–78. 18, 175, 179, 180

Jin, F.-F., 1997: An equatorial ocean recharge paradigm for ENSO. Part I: Conceptual model. *J. Atmos. Sci.*, **54**, 811–829. 144, 175, 178, 185

Jin, F.-F., 2000: Low frequency modes of tropical ocean dynamics. *J. Climate*, **14**, 3874–3881. 12

Jin, F.-F., Z.-Z. Hu, M. Latif, L. Bengtsson, and E. Roeckner, 2001: Dynamical and cloud-radiation feedbacks in El Niño and greenhouse warming. *Geophys. Res. Lett.*, **28**, 1539–1542. 16, 17

Jin, F.-F. and J. D. Neelin, 1993a: Modes of interannual tropical ocean-atmosphere interaction–a unified view. Part I: Numerical results. *J. Atmos. Sci.*, **50**, 3477–3503. 18, 149, 175, 177, 179, 181

Jin, F.-F. and J. D. Neelin, 1993b: Modes of interannual tropical ocean-atmosphere interaction–a unified view. Part III: Analytical results in fully coupled cases. *J. Atmos. Sci.*, **50**, 3523–3540. 18, 175, 181

Jin, F.-F., J. D. Neelin, and M. Ghil, 1994: El Niño on the devil's staircase: Annual subharmonic steps to chaos. *Science*, **264**, 70–72. 129

Johnson, G. C. and M. J. McPhaden, 1999: Interior pycnocline flow from the subtropical to the equatorial Pacific ocean. *J. Phys. Oceanogr.*, **29**, 3073–3089. 12

Johnson, G. C., M. J. McPhaden, and E. Firing, 2001: Equatorial Pacific ocean horizontal velocity, divergence, and upwelling. *J. Phys. Oceanogr.*, **31**, 839–849. 97

Jones, P. D., T. J. Osborn, and K. R. Briffa, 2001: The evolution of climate over the last millennium. *Science*, **292**, 662–667. 14

Kachi, M. and T. Nitta, 1997: Decadal variations of the global atmosphere-ocean system. *J. Meteor. Soc. Japan*, **75**, 657–675. 12

Kalnay, E., M. Kanamitsu, R. Kistler, and Coauthors, 1996: The NCEP/NCAR 40-year reanalysis project. *Bull. Amer. Meteor. Soc.*, **77**, 437–471. 25, 101

Kang, I.-S. and S.-I. An, 1998: Kelvin and Rossby wave contributions to the SST oscillation of ENSO. *J. Climate*, **11**, 2461–2469. 86, 93

Kang, I.-S., S.-I. An, and F.-F. Jin, 2001: A systematic approximation of the SST anomaly equation for ENSO. *J. Meteor. Soc. Japan*, **79**, 1–10. 113

Kang, I.-S. and J.-S. Kug, 2000: An El Niño prediction system using an intermediate ocean and a statistical atmosphere. *Geophys. Res. Lett.*, **27**, 1167–1170. 56

Kang, I.-S. and J.-S. Kug, 2002: El Niño and La Niña sea surface temperature anomalies: Asymmetry characteristics associated with their wind stress anomalies. *J. Geophys. Res.*, **107**, doi:10.1029/2001JD000393. 38

Kaplan, A., M. A. Cane, Y. Kushnir, A. C. Clement, M. B. Blumenthal, and B. Rajagopalan, 1998: Analyses of global sea surface temperature 1856–1991. *J. Geophys. Res.*, **103**, 18 567–18 589. 11, 161

Kelly, K. A., S. Dickinson, M. J. McPhaden, and G. C. Johnson, 2001: Ocean currents evident in satellite wind data. *Geophys. Res. Lett.*, **28**, 2469–2472. 22

Kelly, K. A., S. Dickinson, and Z. Yu, 1999: NSCAT tropical wind stress maps: Implications for improving ocean modeling. *J. Geophys. Res.*, **104**, 11 291–11 310. 24

Kerr, R. A., 1993: El Niño metamorphosis throws forecasters. *Science*, **262**, 656–657. 4, 13

Kerr, R. A., 1999a: Big El Niños ride the back of slower climate change. *Science*, **283**, 1108–1109. 12

Kerr, R. A., 1999b: El Niño grew strong as cultures were born. *Science*, **283**, 467–468. 14

Kerr, R. A., 2000a: Globe's "missing warming" found in the ocean. *Science*, **287**, 2126–2127. 10

Kerr, R. A., 2000b: Second thoughts on skill of El Niño predictions. *Science*, **290**, 257–258. 4

Kestin, T. S., D. J. Karoly, J.-I. Yano, and N. A. Rayner, 1998: Time-frequency variability of ENSO and stochastic simulations. *J. Climate*, **11**, 2258–2272. 13, 14

Kirtman, B. P., 1997: Oceanic Rossby wave dynamics and the ENSO period in a coupled model. *J. Climate*, **10**, 1690–1704. 22, 38, 56

Kirtman, B. P. and E. K. Schneider, 1996: Model-based estimates of equatorial Pacific wind stress. *J. Climate*, **9**, 1077–1091. 23

Kirtman, B. P. and P. S. Schopf, 1998: Decadal variability in ENSO predictability and prediction. *J. Climate*, **11**, 2804–2822. 4, 14, 18, 22

Kleeman, R., 1991: A simple model of the atmospheric response to ENSO sea surface temperature anomalies. *J. Atmos. Sci.*, **48**, 3–18. 40

Kleeman, R., 1993: On the dependence of hindcast skill on ocean thermodynamics in a coupled ocean-atmosphere model. *J. Climate*, **6**, 2012–2033. 92

Kleeman, R., R. A. Colman, N. R. Smith, and S. B. Power, 1996: A recent change in the mean state of the Pacific basin climate: Observational evidence and atmospheric and oceanic responses. *J. Geophys. Res.*, **101**, 20 483–20 499. 12, 13

Kleeman, R., J. P. McCreary, and B. A. Klinger, 1999: A mechanism for generating ENSO decadal variability. *Geophys. Res. Lett.*, **26**, 1743–1746. 12, 14, 26

Kleeman, R. and A. M. Moore, 1997: A theory for the limitation of ENSO predictability due to stochastic atmospheric transients. *J. Atmos. Sci.*, **54**, 753–767. 22

Kleeman, R., G. Wang, and S. Jewson, 2001: Surface flux response to interannual tropical Pacific sea surface temperature variability in AMIP models. *Climate Dyn.*, **17**, 627–641. 8, 24, 25, 56

Knaff, J. A. and C. W. Landsea, 1997: An El Niño-Southern Oscillation climatology and persistence (CLIPER) forecasting scheme. *Wea. Forecasting*, **12**, 633–652. 4

Knutson, T. R. and S. Manabe, 1995: Time-mean response over the tropical Pacific to increased CO_2 in a coupled ocean-atmosphere model. *J. Climate*, **8**, 2181–2199. 16

Knutson, T. R. and S. Manabe, 1998: Model assessment of decadal variability and trends in the tropical Pacific ocean. *J. Climate*, **11**, 2273–2296. 12, 16

Knutson, T. R., S. Manabe, and D. Gu, 1997: Simulated ENSO in a global coupled ocean-atmosphere model: Multidecadal amplitude modulation and CO_2 sensitivity. *J. Climate*, **10**, 138–161. 17

Kug, J.-S., I.-S. Kang, and S. E. Zebiak, 2001: The impacts of the model assimilated wind stress data in the initialization of an intermediate ocean and the ENSO predictability. *Geophys. Res. Lett.*, **28**, 3713–3716. 24

Lagerloef, G. S. E., G. T. Mitchum, R. B. Lukas, and P. P. Niiler, 1999: Tropical Pacific near-surface currents estimated from altimeter, wind, and drifter data. *J. Geophys. Res.*, **104**, 23 313–23 326. 93

Landsea, C. W. and J. A. Knaff, 2000: How much skill was there in forecasting the very strong 1997–98 El Niño? *Bull. Amer. Meteor. Soc.*, **81**, 2107–2119. 4, 5, 56, 82, 131

Landsteiner, M. C., M. J. McPhaden, and J. Picaut, 1990: On the sensitivity of Sverdrup transport estimates to the specification of wind stress forcing in the tropical Pacific. *J. Geophys. Res.*, **95**, 1681–1691. 22, 24

Latif, M., 1987: Tropical ocean circulation experiments. *J. Phys. Oceanogr.*, **17**, 246–263. 22, 24

Latif, M., 1998: Dynamics of interdecadal variability in coupled ocean-atmosphere models. *J. Climate*, **11**, 602–624. 12

Latif, M. and M. Flügel, 1991: An investigation of short-range climate predictability of the El Niño/Southern Oscillation in the tropical Pacific. *J. Geophys. Res.*, **96**, 2661–2673. 131, 132

Latif, M., R. Kleeman, and C. Eckert, 1997: Greenhouse warming, decadal variability, or El Niño? An attempt to understand the anomalous 1990s. *J. Climate*, **10**, 2221–2239. 13, 14, 45

Latif, M., K. Sperber, and CMIP participants, 2001: ENSIP: The El Niño Simulation Intercomparison Project. *Climate Dyn.*, **18**, 255–276. 4, 8, 9, 56

Latif, M., et al., 1998: A review of the predictability and prediction of ENSO. *J. Geophys. Res.*, **103**, 14 375–14 393. 3, 4

Lau, K. M., C.-H. Sui, M.-D. Chou, and W. K. Tao, 1994: An inquiry into the cirrus-cloud thermostat effect for tropical sea surface temperature. *Geophys. Res. Lett.*, **21**, 1157–1160. 16

Lau, K.-M. and H. Weng, 1995: Climate signal detection using wavelet transform: How to make a time series sing. *Bull. Amer. Meteor. Soc.*, **76**, 2391–2402. 45

Lau, K.-M. and H. Weng, 1999: Interannual, decadal-interdecadal, and global warming signals in sea surface temperature during 1955–97. *J. Climate*, **12**, 1257–1267. 12

Lea, D. W., D. K. Pak, and H. J. Spero, 2000: Climate impact of late quaternary equatorial Pacific sea surface temperature variations. *Science*, **2000**, 1719–1724. 15

Legler, D. M. and J. J. O'Brien, 1988: Tropical Pacific wind stress analysis for TOGA, IOC Time series of ocean measurements. IOC Technical Series 33, UNESCO. 25

Levitus, S., J. I. Antonov, T. P. Boyer, and C. Stephens, 2000: Warming of the world ocean. *Science*, **287**, 2225–2229. 10

Levitus, S. and T. P. Boyer, 1994: World Ocean Atlas 1994 Volume 4: Temperature. NOAA Atlas NESDIS 4, U.S. Department of Commerce, Washington, D.C. 263

Li, T., 1997: Phase transition of the El Niño-Southern Oscillation: A stationary SST mode. *J. Atmos. Sci.*, **54**, 2872–2887. 175

Li, T. and T. F. Hogan, 1999: The role of the annual-mean climate on seasonal and interannual variability of the tropical Pacific in a coupled GCM. *J. Climate*, **12**, 780–792. 149, 181, 188

Li, T. and S. G. H. Philander, 1996: On the annual cycle of the eastern equatorial Pacific. *J. Climate*, **9**, 2986–2998. 149

Lindzen, R. S. and S. Nigam, 1987: On the role of sea surface temperature gradients in forcing low-level winds and convergence in the tropics. *J. Atmos. Sci.*, **44**, 2418–2436. 23, 29

Linsley, B. K., G. M. Wellington, and D. P. Schrag, 2000: Decadal sea surface temperature variability in the subtropical south Pacific from 1726 to 1997 A.D. *Science*, **290**, 1145–1148. 12

Liu, W. T. and C. Gautier, 1990: Thermal forcing on the tropical Pacific from satellite data. *J. Geophys. Res.*, **95**, 13 209–13 217. 99

Liu, Z., 1998: The role of ocean in the response of tropical climatology to global warming: The west-east SST contrast. *J. Climate*, **11**, 864–875. 16

Liu, Z. and B. Huang, 1997: A coupled theory of tropical climatology: warm pool, cold tongue, and Walker Circulation. *J. Climate*, **10**, 1662–1679. 16

Liu, Z. and B. Huang, 2000: Cause of tropical Pacific warming trend. *Geophys. Res. Lett.*, **27**, 1935–1938. 10

Liu, Z., J. Kutzbach, and L. Wu, 2000a: Modeling climate shift of El Niño variability in the Holocene. *Geophys. Res. Lett.*, **27**, 2265–2268. 14, 15

Liu, Z., S. Shin, P. Behling, W. Prell, M. Trend-Staid, S. P. Harrison, and J. Kutzbach, 2000b: Dynamical and observational constraints on tropical Pacific sea surface temperatures at the last glacial maximum. *Geophys. Res. Lett.*, **27**, 105–108. 15

Liu, Z. and R.-H. Zhang, 1999: Propagation and mechanism of decadal upper-ocean variability in the north Pacific. *Geophys. Res. Lett.*, **26**, 739–742. 12

Lorenz, E. N., 1963: Deterministic nonperiodic flow. *J. Atmos. Sci.*, **20**, 130–141. 2

Lorenz, E. N., 1975: Climatic predictability. *The Physical Basis of Climate and Climate Modelling*, World Meteorological Organization, Geneva, Switzerland, No. 16 in Global Atmospheric Research Programme Publication Series, 132–136, report of the International Study Conference in Stockholm, 29 July – 10 August 1974. 2

Manabe, S. and R. J. Stouffer, 1988: Two stable equilibria of a coupled ocean-atmosphere model. *J. Climate*, **1**, 841–866. 173

Mann, M. E., R. S. Bradley, and M. K. Hughes, 2000: Long-term variability in the El Niño Southern Oscillation and associated teleconnections. *El Niño and the Southern Oscillation: Multiscale variability and its impacts on natural ecosystems and society*, H. F. Diaz and V. Markgraf, Eds., Cambridge University Press, Cambridge, United Kingdom, 357–412. 14

Mann, M. E. and J. Park, 1994: Global-scale modes of surface temperature variability on interannual to century timescales. *J. Geophys. Res.*, **99**, 25 819–25 833. 12, 13

Mantua, N. J. and D. S. Battisti, 1994: Evidence for the delayed oscillator mechanism for ENSO: The "observed" oceanic Kelvin mode in the western Pacific. *J. Phys. Oceanogr.*, **24**, 691–699. 86, 93

Mantua, N. J. and D. S. Battisti, 1995: Aperiodic variability in the Zebiak-Cane coupled ocean-atmosphere model: Air-sea interactions in the western equatorial Pacific. *J. Climate*, **8**, 2897–2927. 91, 92, 177

Masina, S. and S. G. H. Philander, 1999a: An analysis of tropical instability waves in a numerical model of the Pacific ocean. 1. Spatial variability of the waves. *J. Geophys. Res.*, **104**, 29 613–29 635. 269

Masina, S. and S. G. H. Philander, 1999b: An analysis of tropical instability waves in a numerical model of the Pacific ocean. 2. Generation and energetics of the waves. *J. Geophys. Res.*, **104**, 29 637–29 661. 269

McCreary, J. P. and D. L. T. Anderson, 1991: An overview of coupled ocean-atmosphere models of El Niño and the Southern Oscillation. *J. Geophys. Res.*, **Feb. 1996 Suppl.**, 3125–3150. 19

McPhaden, M. J., A. J. Busalacchi, and J. Picaut, 1988: Observations and wind-forced model simulations of the mean seasonal cycle in tropical Pacific sea surface topography. *J. Geophys. Res.*, **93**, 8131–8146. 22, 24, 29

McPhaden, M. J. and D. Zhang, 2002: Slowdown of the meridional overturning circulation in the upper Pacific ocean. *Nature*, **415**, 603–608. 10, 13

McPhaden, M. J., et al., 1998: The Tropical Ocean-Global Atmosphere observing system: A decade of progress. *J. Geophys. Res.*, **103**, 14 169–14 240. 3, 22, 40, 56, 91, 269

Mechoso, C. R., A. W. Robertson, and Coauthors, 1995: The seasonal cycle over the tropical Pacific in coupled ocean-atmosphere general circulation models. *Mon. Wea. Rev.*, **123**, 2825–2838. 8

Meehl, G. A., G. J. Boer, C. Covey, M. Latif, and R. J. Stouffer, 2000a: The Coupled Model Intercomparison Project (CMIP). *Bull. Amer. Meteor. Soc.*, **81**, 313–318. 16

Meehl, G. A., G. W. Branstator, and W. M. Washington, 1993: Tropical Pacific interannual variability and CO_2 climate change. *J. Climate*, **6**, 42–63. 17

Meehl, G. A., W. D. Collins, B. Boville, J. T. Kiehl, T. M. L. Wigley, and J. M. Arblaster, 2000b: Response of the NCAR Climate System model to increased CO_2 and the role of physical processes. *J. Climate*, **13**, 1879–1898. 16

Meehl, G. A., P. R. Gent, J. M. Arblaster, B. L. Otto-Bliesner, E. C. Brady, and A. Craig, 2001a: Factors that affect the amplitude of El Niño in global coupled climate models. *Climate Dyn.*, **17**, 515–526. 8

Meehl, G. A., R. Lukas, G. N. Kiladis, K. M. Weickmann, A. J. Matthews, and M. Wheeler, 2001b: A conceptual framework for time and space scale interactions in the climate system. *Climate Dyn.*, **17**, 753–775. 48

Meehl, G. A. and W. M. Washington, 1996: El Niño-like climate change in a model with increased atmospheric CO_2 concentrations. *Nature*, **382**, 56–60. 16

Mehta, V., E. Lindstrom, and Coauthors, 2000: Proceedings of the NASA Workshop on Decadal Climate Variability. *Bull. Amer. Meteor. Soc.*, **81**, 2983–2985. 10, 13

Meinen, C. S., M. J. McPhaden, and G. C. Johnson, 2001: Vertical velocities and transports in the equatorial Pacific during 1993–99. *J. Phys. Oceanogr.*, **31**, 3230–3248. 97

Meissner, T., D. Smith, and F. Wentz, 2001: A 10 year intercomparison between collocated Special Sensor Microwave Imager oceanic surface wind speed retrievals and global analyses. *J. Geophys. Res.*, **106**, 11 731–11 742. 24

Mestas-Nuñez, A. M. and D. B. Enfield, 2001: Eastern equatorial Pacific SST variability: ENSO and non-ENSO components and their climatic associations. *J. Climate*, **14**, 391–402. 12

Michaud, R. and C. A. Lin, 1992: Monthly summaries of merchant ship surface marine observations and implications for climate variability studies. *Climate Dyn.*, **7**, 45–55. 22

Moore, A. M., 1995: Tropical interannual variability in a global coupled GCM: sensitivity to mean climate state. *J. Climate*, **8**, 807–828. 18, 181, 187

Moore, A. M. and R. Kleeman, 1996: The dynamics of error growth and predictability in a coupled model of ENSO. *Quart. J. Roy. Meteor. Soc.*, **122**, 1405–1446. 81, 131

Moore, A. M. and R. Kleeman, 1997a: The singular vectors of a coupled ocean-atmosphere model of ENSO. Part I: Thermodynamics, energetics and error growth. *Quart. J. Roy. Meteor. Soc.*, **123**, 953–981. 81, 131

Moore, A. M. and R. Kleeman, 1997b: The singular vectors of a coupled ocean-atmosphere model of ENSO. Part II: Sensitivity studies and dynamical interpretation. *Quart. J. Roy. Meteor. Soc.*, **123**, 983–1006. 81, 131

Moore, A. M. and R. Kleeman, 1998: Skill assessment for ENSO using ensemble prediction. *Quart. J. Roy. Meteor. Soc.*, **124**, 557–584. 81, 131

Moore, A. M. and R. Kleeman, 2001: The differences between the optimal perturbations of coupled models of ENSO. *J. Climate*, **14**, 138–163. 81, 131

Moron, V., R. Vautard, and M. Ghil, 1998: Trends, interdecadal and interannual oscillations in global sea-surface temperatures. *Climate Dyn.*, **14**, 545–569. 12

Morrissey, M. L., 1990: An evaluation of ship data in the equatorial western Pacific. *J. Climate*, **3**, 99–112. 22

Murphy, J. M., 1988: The impact of ensemble forecasts on predictability. *Quart. J. Roy. Meteor. Soc.*, **114**, 463–493. 132

National Research Council, (Ed.) , 1995: *Natural climate variability on decade-to-century time scales*. National Academy Press, Washington, D.C., 630pp. 10

Navarra, A., (Ed.) , 1999: *Beyond El Niño: Decadal and interdecadal climate variability*. Springer-Verlag, Berlin, Germany, 374pp. 10

Neelin, J. D., 1990: A hybrid coupled general circulation model for El Niño studies. *J. Atmos. Sci.*, **47**, 674–693. 22, 38, 56

Neelin, J. D., 1991: The slow sea surface temperature mode and the fast-wave limit: Analytic theory for tropical interannual oscillations and experiments in a hybrid coupled model. *J. Atmos. Sci.*, **48**, 584–606. 18, 175, 177, 181, 187, 202

Neelin, J. D., D. S. Battisti, A. C. Hirst, F.-F. Jin, Y. Wakata, T. Yamagata, and S. Zebiak, 1998: ENSO theory. *J. Geophys. Res.*, **103**, 14 261–14 290. 18, 19, 23, 84, 91, 129, 139, 149, 175

Neelin, J. D. and H. A. Dijkstra, 1995: Ocean-atmosphere interaction and the tropical climatology. Part I: The dangers of flux correction. *J. Climate*, **8**, 1325–1342. 153, 260, 261

Neelin, J. D. and F.-F. Jin, 1993: Modes of interannual tropical ocean-atmosphere interaction–a unified view. Part II: Analytical results in the weak-coupling limit. *J. Atmos. Sci.*, **50**, 3504–3522. 18, 181

Neelin, J. D., et al., 1992: Tropical air-sea interaction in general circulation models. *Climate Dyn.*, **7**, 73–104. 8, 187

Newman, M. and P. D. Sardeshmukh, 1995: A caveat concerning singular value decomposition. *J. Climate*, **8**, 352–361. 58, 60

Nitta, T. and S. Yamada, 1989: Recent warming of tropical sea surface temperature and its relationship to the Northern Hemisphere circulation. *J. Meteor. Soc. Japan*, **67**, 375–383. 45

Noda, A., K. Yamaguchi, S. Yamaki, and S. Yukimoto, 1999: Relationship between natural variability and CO_2-induced warming pattern: MRI AOGCM experiment. *10th Symposium on Global Change Studies*, American Meteorological Society, Boston, Massachusetts, 359–362. 16

Nurnberg, D., 2000: Taking the temperature of past ocean surfaces. *Science*, **289**, 1698–1699. 15

Otto-Bliesner, B. L., 1999: El Niño/La Niña and Sahel precipitation during the middle Holocene. *Geophys. Res. Lett.*, **26**, 87–90. 14, 15

Pacanowski, R. C. and S. G. H. Philander, 1981: Parameterization of vertical mixing in numerical models of tropical oceans. *J. Geophys. Res.*, **86**, 1903–1916. 263

Penland, C., 1996: A stochastic model of IndoPacific sea surface temperature anomalies. *Physica D*, **98**, 534–558. 132

Penland, C. and P. D. Sardeshmukh, 1995: The optimal growth of tropical sea surface temperature anomalies. *J. Climate*, **8**, 1999–2024. 22, 81, 129, 132, 197

Perigaud, C. and B. Dewitte, 1996: El Niño – La Niña events simulated with Cane and Zebiak's model and observed with satellite or in situ data. Part I: Model data comparison. *J. Climate*, **9**, 66–84. 91, 92

Perigaud, C., F. Melin, and C. Cassou, 2000a: ENSO simulated by intermediate coupled models and evaluated with observations over 1970–1998. Part I: Role of the off-equatorial variability. *J. Climate*, **13**, 1605–1634. 91

Perigaud, C., S. E. Zebiak, F. Melin, J.-P. Boulanger, and B. Dewitte, 1997: On the role of meridional wind anomalies in a coupled model of ENSO. *J. Climate*, **10**, 761–773. 91

Perigaud, C. M., C. Cassou, B. Dewitte, L.-L. Fu, and J. D. Neelin, 2000b: Using data and intermediate coupled models for seasonal-to-interannual forecasts. *Mon. Wea. Rev.*, **128**, 3025–3049. 181

Peterson, E. Q. and L. Hasse, 1987: Did the Beaufort scale or the wind climate change? *J. Phys. Oceanogr.*, **17**, 1071–1074. 22

Philander, S. G., 1990: *El Niño, La Niña, and the Southern Oscillation*. Academic Press, San Diego, 293pp. 92, 139, 140

Philander, S. G. H., 1999: A review of tropical ocean-atmosphere interactions. *Tellus*, **51A**, 71–90. 139, 175

Philander, S. G. H., D. Gu, D. Halpern, G. Lambert, N.-C. Lau, T. Li, and R. C. Pacanowski, 1996: Why the ITCZ is mostly north of the equator. *J. Climate*, **9**, 2958–2972. 28, 163

Picaut, J. and T. Delcroix, 1995: Equatorial wave sequence associated with warm pool displacements during the 1986–1989 El Niño-La Niña. *J. Geophys. Res.*, **100**, 18 393–18 408. 116

Picaut, J., F. Masia, and Y. du Penhoat, 1997: An advective-reflective conceptual model for the oscillatory nature of the ENSO. *Science*, **277**, 663–666. 116

Picaut, J., C. Menkes, J.-P. Boulanger, and Y. du Penhoat, 1993: Dissipation in a Pacific equatorial long wave model. *TOGA Notes*, **10**, 11–15. 92

Pierce, D. W., T. P. Barnett, and M. Latif, 2000a: Connections between the Pacific ocean tropics and midlatitudes on decadal timescales. *J. Climate*, **13**, 1173–1194. 13

Pierce, D. W., T. P. Barnett, N. Schneider, R. Saravanan, D. Dommenget, and M. Latif, 2000b: The role of ocean dynamics in producing decadal climate variability in the North Pacific. *Climate Dyn.*, **18**, 51–70. 13

Pierrehumbert, R. T., 1995: Thermostats, radiator fins, and the local runaway greenhouse. *J. Atmos. Sci.*, **52**, 1784–1806. 16

Polito, P. S., J. P. Ryan, W. T. Liu, and F. P. Chavez, 2001: Oceanic and atmospheric anomalies of tropical instability waves. *Geophys. Res. Lett.*, **28**, 2233–2236. 269

Pontaud, M., J.-P. Cerón, M. Kimoto, F. Pluviaud, L. Terray, and A. Vintzileos, 2000: CoPIVEP: A theory-based analysis of coupled processes and interannual variability in the equatorial Pacific in four coupled GCMs. *Climate Dyn.*, **16**, 917–933. 8

Posmentier, E. S., M. A. Cane, and S. E. Zebiak, 1989: Tropical Pacific climate trends since 1960. *J. Climate*, **2**, 731–736. 10, 22

Putman, W. M., D. M. Legler, and J. J. O'Brien, 2000: Interannual variability of synthesized FSU and NCEP-NCAR reanalysis pseudostress products over the Pacific ocean. *J. Climate*, **13**, 3003–3016. 25

Quinn, W. H., V. T. Neal, and S. E. Antunez de Mayolo, 1987: El Niño occurrences over the past four and a half centuries. *J. Geophys. Res.*, **92**, 14 449–14 461. 13

Rajagopalan, B., U. Lall, and M. A. Cane, 1997: Anomalous ENSO occurrences: An alternate view. *J. Climate*, **10**, 2351–2357. 14

Ramage, C. S., 1987: Secular change in reported surface wind speeds over the ocean. *J. Climate Appl. Meteor.*, **26**, 525–528. 22

Ramanathan, V. and W. D. Collins, 1991: Thermodynamic regulation of ocean warming by cirrus clouds deduced from observations of the 1987 El Niño. *Nature*, **351**, 27–32. 16

Rasmusson, E. M. and T. H. Carpenter, 1982: Variations in tropical sea surface temperature and surface wind fields associated with the Southern Oscillation / El Niño. *Mon. Wea. Rev.*, **110**, 354–384. 3

Rasmusson, E. M., X. Wang, and C. F. Ropelewski, 1995: Secular variability of the ENSO cycle. *Natural Climate Variability on Decade-to-Century Time Scales*, National Academy Press, 458–471. 13

Ravelo, A. C. and N. J. Shackleton, 1995: Evidence for surface water circulation changes at site 851 in the eastern tropical pacific ocean. *Proceedings of the Ocean Drilling Program*, N. G. Pisias, L. A. Mayer, T. R. Janecek, A. Palmer-Julson, and T. H. van Andel, Eds., 503–516. 14

Reynolds, R. W., K. Arpe, C. Gordon, S. P. Hayes, A. Leetmaa, and M. J. McPhaden, 1989: A comparison of tropical Pacific surface wind analyses. *J. Climate*, **2**, 105–111. 24

Reynolds, R. W. and T. M. Smith, 1994: Improved global sea surface temperature analyses. *J. Climate*, **7**, 929–948. 11, 37, 265

Rind, D., 1987: The doubled CO_2 climate: Impact of the sea surface temperature gradient. *J. Atmos. Sci.*, **44**, 3235–3268. 17, 145

Rodbell, D. T., G. O. Seltzer, D. M. Anderson, M. B. Abbott, D. B. Enfield, and J. H. Newman, 1999: An ∼15,000-year record of an El Niño-driven alluviation in southwestern Ecuador. *Science*, **283**, 516–520. 14

Roulston, M. S. and J. D. Neelin, 2000: The response of an ENSO model to climate noise, weather noise and intraseasonal forcing. *Geophys. Res. Lett.*, **27**, 3723–3726. 22

Royston, J. P., 1982: Algorithm AS181: The W Test for Normality. *Appl. Statist.*, **31**, 176–180. 72

Saji, N. H. and B. N. Goswami, 1997: Intercomparison of the seasonal cycle of tropical surface stress in 17 AMIP atmospheric general circulation models. *Climate Dyn.*, **13**, 561–585. 24, 25, 56

Samelson, R. M. and E. Tziperman, 2001: Instability of the chaotic ENSO: the growth-phase predictability barrier. *J. Atmos. Sci.*, **58**, 3613–3625. 136

Sandweiss, D. H., J. B. Richardson III, E. J. Reitz, H. B. Rollins, and K. A. Maasch, 1996: Geoarchaeological evidence from Peru for a 5000 years B.P. onset of El Niño. *Science*, **273**, 1531–1533. 14

Sandweiss, D. H., J. B. Richardson III, E. J. Reitz, H. B. Rollins, and K. A. Maasch, 1997: Determining the early history of El Niño. *Science*, **276**, 966–967. 14

Santer, B. D., J. J. Hnilo, T. M. L. Wigley, J. S. Boyle, C. Doutriaux, M. Fiorino, D. E. Parker, and K. E. Taylor, 1999: Uncertainties in "observational" estimates of temperature change in the free atmosphere. *J. Geophys. Res.*, **104**, 6305–6333. 45

Schneider, E. K., 2002: Understanding differences between the equatorial Pacific as simulated by two coupled GCMs. *J. Climate*, **15**, 449–469. 8

Schneider, E. K., B. Huang, and J. Shukla, 1995: Ocean wave dynamics and El Niño. *J. Climate*, **8**, 2415–2439. 175

Schneider, N., A. J. Miller, M. A. Alexander, and C. Deser, 1999a: Subduction of decadal north Pacific temperature anomalies: Observations and dynamics. *J. Phys. Oceanogr.*, **29**, 1056–1070. 12

Schneider, N., S. Venzke, A. J. Miller, D. W. Pierce, T. P. Barnett, C. Deser, and M. Latif, 1999b: Pacific thermocline bridge revisited. *Geophys. Res. Lett.*, **26**, 1329–1332. 13

Schneider, T. and S. M. Griffies, 1999: A conceptual framework for predictability studies. *J. Climate*, **12**, 3133–3155. 132

Schopf, P. S. and M. J. Suarez, 1988: Vacillations in a coupled ocean-atmosphere model. *J. Atmos. Sci.*, **45**, 549–566. 175

Seager, R., 1989: Modeling tropical Pacific sea surface temperature: 1970–87. *J. Phys. Oceanogr.*, **19**, 419–434. 99

Seager, R. and R. Murtugudde, 1997: Ocean dynamics, thermocline adjustment, and regulation of tropical SST. *J. Climate*, **10**, 521–534. 16

Seager, R., S. E. Zebiak, and M. A. Cane, 1988: A model of the tropical Pacific sea surface temperature climatology. *J. Geophys. Res.*, **93**, 1265–1280. 91

Setoh, T., S. Imawaki, A. Ostrovskii, and S.-I. Umatani, 1999: Interdecadal variations of ENSO signals and annual cycles revealed by wavelet analysis. *J. Oceanogr.*, **55**, 385–394. 13

Shinoda, T., H. H. Hendon, and J. Glick, 1999: Intraseasonal surface fluxes in the tropical western Pacific and Indian oceans from NCEP Reanalyses. *Mon. Wea. Rev.*, **127**, 678–693. 24

Silverman, B. W., 1986: *Density Estimation for Statistics and Data Analysis*. Chapman and Hall, 175pp. 49

Smagorinsky, J., 1963: General circulation experiments with the primitive equations. Part I: The basic experiment. *Mon. Wea. Rev.*, **91**, 99–164. 263

Smith, S. D., 1988: Coefficients for sea surface wind stress, heat flux, and wind profiles as a function of wind speed and temperature. *J. Geophys. Res.*, **93**, 15 467–15 472. 22

Smith, S. R., D. M. Legler, and K. V. Verzone, 2001: Quantifying uncertainties in NCEP reanalyses using high-quality research vessel observations. *J. Climate*, **14**, 4062–4072. 24, 25

Smith, T. M., R. W. Reynolds, R. E. Livezey, and D. C. Stokes, 1996: Reconstruction of historical sea surface temperatures using empirical orthogonal functions. *J. Climate*, **9**, 1403–1420. 26, 37

Stahle, D. W., et al., 1998: Experimental dendroclimatic reconstruction of the Southern Oscillation. *Bull. Amer. Meteor. Soc.*, **79**, 2137–2152. 14

Stephens, C., S. Levitus, J. Antonov, and T. P. Boyer, 2001: On the Pacific ocean regime shift. *Geophys. Res. Lett.*, **28**, 3721–3724. 12

Sterl, A., 2001: On the impact of gap-filling algorithms on variability patterns of reconstructed oceanic surface fields. *Geophys. Res. Lett.*, **28**, 2473–2476. 22

Stern, W. and K. Miyakoda, 1995: Feasibility of seasonal forecasts inferred from multiple GCM simulations. *J. Climate*, **8**, 1071–1085. 132

Stewart, G., 1973: *Introduction to Matrix Computations*. Academic Press, 441pp. 59

Stockdale, T. N., A. J. Busalacchi, D. E. Harrison, and R. Seager, 1998: Ocean modeling for ENSO. *J. Geophys. Res.*, **103**, 14 325–14 355. 269

Strang, G., 1988: *Linear algebra and its applications*. Harcourt, Brace, and Jovanovitch, 505pp. 59

Stricherz, J. N., D. M. Legler, and J. J. O'Brien, 1997: TOGA pseudostress atlas 1985–1994. II: Tropical Pacific Ocean. COAPS Tech. Rep. 97-2, COAPS/The Florida State University, 155 pp., Tallahassee, FL. 25, 263

Suarez, M. J. and P. S. Schopf, 1988: A delayed action oscillator for ENSO. *J. Atmos. Sci.*, **45**, 3283–3287. 144, 175

Sun, D.-Z. and Z. Liu, 1996: Dynamic ocean-atmosphere coupling: A thermostat for the tropics. *Science*, **272**, 1148–1150. 16

Syu, H.-H. and J. D. Neelin, 1995: Seasonal and interannual variability in a hybrid coupled GCM. *J. Climate*, **8**, 2121–2143. 56, 61, 73, 82, 253

Takayabu, Y. N., T. Iguchi, M. Kachi, A. Shibata, , and H. Kanzawa, 1999: Abrupt termination of the 1997–98 El Niño in response to a Madden-Julian oscillation. *Nature*, **402**, 297–282. 179

Talley, L. D., 1995: Some advances in understanding of the general circulation of the Pacific Ocean, with emphasis on recent U.S. contributions. *Rev. Geophys.*, **July 1995 Suppl.**, 1335–1352. 12

Taylor, P. K., 2001: Intercomparison and validation of ocean-atmosphere energy flux fields. Joint WCRP/SCOR Working Group on Air-Sea Fluxes Final Report. WMO/TD 1036, WCRP-112, 306 pp., Geneva, Switzerland. 25

Tett, S. F. B., 1995: Simulation of El Niño/Southern Oscillation like variability in a global AOGCM and its response to CO_2 increase. *J. Climate*, **8**, 1473–1502. 16, 17

Thompson, C. J. and D. S. Battisti, 2000: A linear stochastic dynamical model of ENSO. Part I: Model development. *J. Climate*, **13**, 2818–2832. 86, 92, 93, 129

Thompson, C. J. and D. S. Battisti, 2001: A linear stochastic dynamical model of ENSO. Part II: Analysis. *J. Climate*, **14**, 445–466. 19, 129

Timmermann, A., 1999: Detecting the nonstationary response of ENSO to greenhouse warming. *J. Atmos. Sci.*, **56**, 2313–2325. 14, 17

Timmermann, A., 2001: Changes of ENSO stability due to greenhouse warming. *Geophys. Res. Lett.*, **28**, 2061–2064. 17

Timmermann, A. and F.-F. Jin, 2002: A nonlinear mechanism for decadal El Niño amplitude changes. *Geophys. Res. Lett.*, **29**, doi:10.1029/2001GL013369. 14

Timmermann, A., J. Oberhuber, A. Bacher, M. Esch, M. Latif, and E. Roeckner, 1999: Increased El Niño frequency in a climate model forced by future greenhouse warming. *Nature*, **398**, 694–697. 16, 17

Tomita, T., B. Wang, T. Yasunari, and H. Nakamura, 2001: Global patterns of decadal-scale variability observed in sea surface temperature and lower-tropospheric circulation fields. *J. Geophys. Res.*, **106**, 26 805–26 815. 12

Torrence, C. and G. P. Compo, 1999: A practical guide to wavelet analysis. *Bull. Amer. Meteor. Soc.*, **79**, 61–78. 3, 13, 45

Torrence, C. and P. J. Webster, 1998: The annual cycle of persistence in the El Niño/Southern Oscillation. *Quart. J. Roy. Meteor. Soc.*, **124**, 1985–2004. 3, 13, 45

Torrence, C. and P. J. Webster, 1999: Interdecadal changes in the ENSO-monsoon system. *J. Climate*, **12**, 2679–2690. 3, 45

Tourre, Y. M., B. Rajagopalan, Y. Kushnir, M. Barlow, and W. B. White, 2001: Patterns of coherent decadal and interdecadal climate signals in the Pacific basin during the 20th century. *Geophys. Res. Lett.*, **28**, 2069–2072. 12

Trenberth, K. E. and T. J. Hoar, 1996: The 1990–1995 El Niño-Southern Oscillation event: Longest on record. *Geophys. Res. Lett.*, **23**, 57–60. 14

Trenberth, K. E. and T. J. Hoar, 1997: El Niño and climate change. *Geophys. Res. Lett.*, **24**, 3057–3060. 14

Trenberth, K. E. and J. W. Hurrell, 1994: Decadal atmosphere-ocean variations in the Pacific. *Climate Dyn.*, **9**, 303–319. 12, 13, 45

Trenberth, K. E. and J. W. Hurrell, 1999: Comments on "The interpretation of short climate records, with comments on the North Atlantic and Southern Oscillations". *Bull. Amer. Meteor. Soc.*, **80**, 2721–2722. 14

Trenberth, K. E., W. G. Large, and J. G. Olson, 1990: The mean annual cycle in global ocean wind stress. *J. Phys. Oceanogr.*, **20**, 1742–1760. 24

Trenberth, K. E. and D. P. Stepaniak, 2001: Indices of El Niño evolution. *J. Climate*, **14**, 1697–1701. 13, 66

Tudhope, A. W., et al., 2001: Variability in the El Niño-Southern Oscillation through a glacial-interglacial cycle. *Science*, **291**, 1511–1517. 2, 14, 15

Tziperman, E., M. A. Cane, and S. E. Zebiak, 1995: Irregularity and locking to the seasonal cycle in an ENSO prediction model as explained by the quasi-periodicity route to chaos. *J. Atmos. Sci.*, **52**, 293–306. 129

Tziperman, E., M. A. Cane, and S. E. Zebiak, 1997: Mechanisms of seasonal–ENSO interaction. *J. Atmos. Sci.*, **54**, 61–71. 28

Urban, F. E., J. E. Cole, and J. T. Overpeck, 2000: Influence of mean climate change on climate variability from a 155-year tropical Pacific coral record. *Nature*, **407**, 989–993. 10

van den Dool, H. M., 1994: Searching for analogues, how long must we wait? *Tellus*, **46A**, 314–324. 82

van Oldenborgh, G. J., 2000: What caused the onset of the 1997–1998 El Niño? *Mon. Wea. Rev.*, **128**, 2601–2607. 131

Vimont, D. J., D. S. Battisti, and A. C. Hirst, 2002: Pacific interannual and interdecadal equatorial variability in a 1000-yr simulation of the CSIRO coupled general circulation model. *J. Climate*, **15**, 160–178. 12

Wakata, Y. and E. S. Sarachik, 1991: Unstable coupled atmosphere-ocean basin modes in the presence of a spatially varying basic state. *J. Atmos. Sci.*, **48**, 2060–2077. 18, 179

Wakata, Y. and E. S. Sarachik, 1992: Effects of the meridional extent of mean equatorial upwelling on atmosphere-ocean coupled instabilities over an unbounded ocean. *J. Meteor. Soc. Japan*, **70**, 843–854. 18, 179

Wallace, J. M., E. M. Rasmusson, T. P. Mitchell, V. E. Kousky, E. S. Sarachik, and H. von Storch, 1998: On the structure and evolution of ENSO-related climate variability in the tropical Pacific: Lessons from TOGA. *J. Geophys. Res.*, **103**, 14 241–14 259. 10

Wang, B., 1995: Interdecadal changes in El Niño onset in the last four decades. *J. Climate*, **8**, 267–285. 13, 66, 91

Wang, B. and S.-I. An, 2001: Why the properties of El Niño changed during the late 1970s. *Geophys. Res. Lett.*, **28**, 3709–3712. 13, 180

Wang, B. and S.-I. An, 2002: A mechanism for decadal changes of ENSO behavior: Roles of background wind changes. *Climate Dyn.*, **18**, 475–486. 13, 18, 45, 180

Wang, B. and Z. Fang, 1996: Chaotic oscillations of tropical climate: A dynamic system theory for ENSO. *J. Atmos. Sci.*, **53**, 2786–2802. 180

Wang, B. and Z. Fang, 2000: Impacts of shortwave radiation forcing on ENSO: A study with a coupled tropical ocean-atmosphere model. *Climate Dyn.*, **16**, 677–691. 180

Wang, B. and T. Li, 1993: A simple tropical atmosphere model of relevance to short-term climate variations. *J. Atmos. Sci.*, **50**, 260–284. 29, 40

Wang, B. and Y. Wang, 1996: Temporal structure of the Southern Oscillation as revealed by waveform and wavelet analysis. *J. Climate*, **9**, 1586–1598. 3, 13, 45

Wang, B. and Y. Wang, 1999: Dynamics of the ITCZ-equatorial cold tongue complex and causes of the latitudinal climate asymmetry. *J. Climate*, **12**, 1830–1847. 149, 163

Wang, B. and X. Xie, 1996: Low-frequency equatorial waves in vertically sheared zonal flow. Part I: Stable waves. *J. Atmos. Sci.*, **53**, 449–467. 178

Wang, C., 2000a: On the atmospheric responses to tropical Pacific heating during the mature phase of ENSO. *J. Atmos. Sci.*, **57**, 3767–3781. 28

Wang, C., 2001a: A unified oscillator model for the El Niño-Southern Oscillation. *J. Climate*, **14**, 98–115. 19

Wang, C., 2001b: On the ENSO mechanisms. *Adv. Atmos. Sci.*, **18**, 674–691. 19

Wang, W., 2000b: The surface-layer heat balance in the equatorial Pacific ocean. Part II: Interannual variability. *J. Phys. Oceanogr.*, **30**, 2989–3008. 93

Wang, W. and M. J. McPhaden, 2001: Surface layer temperature balance in the equatorial Pacific during the 1997–98 El Niño and 1998–99 La Niña. *J. Climate*, **14**, 3393–3407. 93

Ward, N. M., 1992: Provisionally corrected surface wind data, worldwide ocean-atmosphere surface fields, and Sahelian rainfall variability. *J. Climate*, **5**, 454–475. 22, 23

Ward, N. M. and B. J. Hoskins, 1996: Near-surface wind over the global ocean 1949–1988. *J. Climate*, **9**, 1877–1895. 23

Washington, W. M., et al., 2000: Parallel climate model (PCM) control and transient simulations. *Climate Dyn.*, **16**, 755–774. 16

Weaver, A. J., 1999: Extratropical subduction and decadal modulation of El Niño. *Geophys. Res. Lett.*, **26**, 743–746. 12, 13

Weisberg, R. H. and L. Qiao, 2000: Equatorial upwelling in the central Pacific estimated from moored velocity profilers. *J. Phys. Oceanogr.*, **30**, 105–124. 97

Wells, L. E. and J. S. Noller, 1997: Determining the early history of El Niño. *Science*, **276**, 966. 14

White, W. B. and D. R. Cayan, 1998: Quasi-periodicity and global symmetries in interdecadal upper ocean temperature variability. *J. Geophys. Res.*, **103**, 21 335–21 354. 12

Wielicki, B. A., et al., 2002: Evidence for large decadal variability in the tropical mean radiative energy budget. *Science*, **295**, 841–844. 12

Wilks, D. S., 1995: *Statistical methods in the atmospheric sciences*. Academic Press, San Diego, 467pp. 256

Wright, D. G. and K. R. Thompson, 1983: Time-averaged forms of the nonlinear stress law. *J. Phys. Oceanogr.*, **13**, 341–345. 22

Wright, P. B., 1988: On the reality of climatic changes in wind over the Pacific. *J. Climatol.*, **8**, 521–527. 10, 22

Wu, L., Z. Liu, and H. E. Hurlburt, 2000: Kelvin wave and Rossby wave interaction in the extratropical-tropical Pacific. *Geophys. Res. Lett.*, **27**, 1259–1262. 13

Wunsch, C., 1999: The interpretation of short climate records, with comments on the North Atlantic and Southern Oscillations. *Bull. Amer. Meteor. Soc.*, **80**, 245–255. 14

Wyrtki, K., 1985: Water displacements in the Pacific and the genesis of El Niño cycles. *J. Geophys. Res.*, **90**, 7129–7132. 175

Xie, S.-P., 1994: On the genesis of the equatorial annual cycle. *J. Climate*, **7**, 2008–2013. 188

Yamagata, T. and S. G. H. Philander, 1985: The role of damped equatorial waves in the oceanic response to winds. *J. Oceanogr. Soc. Japan*, **41**, 345–357. 92, 139, 163

Yang, F., A. Kumar, and W. Wang, 2001: Seasonal dependence of surface wind stress variability on SST and precipitation over the tropical Pacific. *Geophys. Res. Lett.*, **28**, 3171–3174. 24, 38

Yang, J., 1991: A coupled atmosphere-ocean model in the tropics with various climatological backgrounds. Ph.D. thesis, Florida State University, 140pp. 178

Yang, J. and J. O'Brien, 1993: A coupled atmosphere-ocean model in the tropics with different thermocline profiles. *J. Climate*, **6**, 1027–1040. 18, 178

Yang, J. and L. Yu, 1992: Propagation of equatorially trapped waves on a sloping thermocline. *J. Phys. Oceanogr.*, **22**, 573–582. 178

Yang, Y. J., T. Y. Tang, and R. H. Weisberg, 1997: Basin-wide zonal wind stress and ocean thermal variations in the equatorial Pacific ocean. *J. Geophys. Res.*, **102**, 911–927. 24

Yu, B. and G. J. Boer, 2002: The roles of radiation and dynamical processes in the El Niño-like response to global warming. *Climate Dyn.*, **19**, 539–553. 16, 17

Yu, Z. and D. W. Moore, 2000: Validating the NSCAT winds in the vicinity of the Pacific Intertropical Convergence Zone. *Geophys. Res. Lett.*, **27**, 2121–2124. 24

Yukimoto, S., M. Endoh, and A. Noda, 2000: ENSO-like interdecadal variability in the Pacific ocean as simulated in a coupled general circulation model. *J. Geophys. Res.*, **105**, 13 945–13 963. 12

Zebiak, S. E., 1985: Tropical atmosphere-ocean interaction and the El Niño / Southern Oscillation phenomenon. Ph.D. thesis, Massachusetts Institute of Technology, 261pp. 90, 175

Zebiak, S. E., 1986: Atmospheric convergence feedback in a simple model for El Niño. *Mon. Wea. Rev.*, **114**, 1263–1271. 82

Zebiak, S. E., 1990: Diagnostic studies of Pacific surface winds. *J. Climate*, **3**, 1016–1031. 23

Zebiak, S. E. and M. A. Cane, 1987: A model El Niño-Southern Oscillation. *Mon. Wea. Rev.*, **115**, 2262–2278. 28, 87, 90, 92, 93, 95, 97, 132, 136, 138, 177, 178, 180

Zhang, C., 2001: Intraseasonal perturbations in sea surface temperatures of the equatorial eastern Pacific and their association with the Madden-Julian Oscillation. *J. Climate*, **14**, 1309–1322. 269

Zhang, C., H. H. Hendon, W. S. Kessler, and A. J. Rosati, 2001a: A workshop on the MJO and ENSO. *Bull. Amer. Meteor. Soc.*, **82**, 971–976. 76

Zhang, R.-H., 1998: Decadal variability of temperature at a depth of 400 meters in the north Pacific ocean. *Geophys. Res. Lett.*, **25**, 1197–1200. 12

Zhang, R.-H., T. Kagimoto, and S. E. Zebiak, 2001b: Subduction of decadal north Pacific thermal anomalies in an ocean GCM. *Geophys. Res. Lett.*, **28**, 2449–2452. 12

Zhang, R.-H. and Z. Liu, 1999: Decadal thermocline variability in the north Pacific ocean: Two pathways around the subtropical gyre. *J. Climate*, **12**, 3273–3296. 12

Zhang, R.-H., L. M. Rothstein, and A. J. Busalacchi, 1998: Origin of upper-ocean warming and El Niño change on decadal scales in the tropical Pacific ocean. *Nature*, **391**, 879–882. 12

Zhang, R.-H., L. M. Rothstein, and A. J. Busalacchi, 1999: Interannual and decadal variability of the subsurface thermal structure in the Pacific ocean: 1961–90. *Climate Dyn.*, **15**, 703–717. 12

Zhang, Y., J. M. Wallace, and D. S. Battisti, 1997: ENSO-like interdecadal variability: 1900–93. *J. Climate*, **10**, 1004–1020. 12